DELLONG David (Orcid ID: 0000-0002-0595-0174)

Klingelhoefer Frauke (Orcid ID: 0000-0001-5838-0577)

Dannowski Anke (Orcid ID: 0000-0001-8581-7500)

Kopp Heidrun (Orcid ID: 0000-0002-6898-1568)

Margheriti Lucia (Orcid ID: 0000-0003-3853-254X)

Moretti Milena (Orcid ID: 0000-0003-0260-6869)

Barreca Giovanni (Orcid ID: 0000-0001-7424-249X)

Scarfì Luciano (Orcid ID: 0000-0002-5995-3880)

# Geometry of the deep Calabrian subduction (Central Mediterranean Sea) from wide-angle seismic data and 3-D gravity modeling.

David Dellong[1,4], Frauke Klingelhoefer[1], Anke Dannowski[2], Heidrun Kopp[2,3], Shane Murphy[1], David Graindorge[4], Lucia Margheriti[5], Milena Moretti[5], Giovanni Barreca[6], Luciano Scarfì[7], Alina Polonia[8], Marc-Andre Gutscher[4]

(1) Géosciences Marines, IFREMER, Centre de Brest, Plouzané, France, (2) GEOMAR, Kiel, Germany, (3) Christian Albrechts University, Kiel, Germany (4) UMR LGO, University of Western Brittany, Brest, France (5) Istituto Nazionale di Geofisica e Vulcanologia (INGV)-Centro Nazionale Terremoti, Rome, Italy (6) Dipartimento di Scienze Biologiche, Geologiche ed Ambientali, University of Catania, Catania, Italy (7) Istituto Nazionale di Geofisica e Vulcanologia (INGV)- Osservatorio Etneo, Catania, Italy (8) ISMAR CNR, Bologna, Italy



This article has been accepted for publication and undergone full peer review but has not been through the copyediting, typesetting, pagination and proofreading process which may lead to differences between this version and the Version of Record. Please cite this article as doi: 10.1029/2019GC008586

**Abstract**

The Calabrian subduction zone is one of the narrowest arcs on Earth and a key area to understand the geodynamic evolution of the Mediterranean and other marginal seas. Here in the Ionian Sea, the African plate subducts beneath Eurasia. Imaging the boundary between the downgoing slab and the upper plate along the Calabrian subduction zone is important for assessing the potential of the subduction zone to generate mega-thrust earthquakes and was the main objective of this study. Here we present and analyze the results from a 380 km long, wide-angle seismic profile spanning the complete subduction zone, from the deep Ionian Basin and the accretionary wedge to NE Sicily, with additional constraints offered by 3-D Gravity modeling and the analysis of earthquake hypocenters. The velocity model for the wide-angle seismic profile images thin oceanic crust throughout the basin. The Calabrian backstop extends underneath the accretionary wedge to about 100 km SE of the coast. The seismic model was extended in depth using earthquake hypocenters. The combined results indicate that the slab dip increases abruptly from 2-3° to 60-70° over a distance of ≤50 km underneath the Calabrian backstop. This abrupt steepening is likely related to the roll-back geodynamic evolution of the narrow Calabrian slab which shows great similarity to the shallow and deep geometry of the Gibraltar slab.

**Plain language abstract**

We investigate the deep crustal structure of southern Italy and the Central Mediterranean where some of the oldest oceanic crust on Earth is actively descending (subducting) into the earth's interior (Speranza et al., 2012). This process causes much of the moderate seismicity observed in this region and may be responsible for strong historical earthquakes as well (Gutscher et al., 2006). Deep seismic data recorded during a marine geophysical expedition performed in 2014, allow us to reconstruct the 3-D geometry of this subduction zone. Our data reveal a 1-4 km thick evaporitic (salt bearing) layer in the 13 km thick accretionary wedge. The thin underlying crust has characteristics of oceanic crust. The adjacent onshore domains (E Sicily and SW Calabria) are composed of 25-30 km thick crust with velocities typical of continental crust. Together with earthquake travel-time tomography (providing images of the subducting slab down to 300 km) and gravity modeling we can for the first time image the abrupt steepening of the subducting slab, the "slab hinge", where slab dip increases from ≤5° to >60° over a downdip distance of 50 km. This slab dip is steep compared to other subduction zones, for example in Northern Honshu Japan or Sumatra, where the slab dip remains roughly 10° down to 40 km depth and therefore may have consequences on the seismicity of the region.

## 1 Introduction

The Calabrian arc is one of the narrowest subduction zones in the world. Here, the African plate subducts towards the NW beneath the Calabrian and Peloritan continental blocks. The forearc region is characterized by moderate seismicity with rare strong events (Scarfi et al., 2013; Carminati et al., 2005). Southern Italy has repeatedly been struck by strong earthquakes that also triggered tsunami (e.g. Messina M7.1 in 1908; Hyblean earthquake M7.5 1693 - Piatanesi & Tinti, 1998; Jacques et al., 2001; Gutscher et al., 2006). The seismicity of the slab is distributed along a well-defined Wadati-Benioff zone with focal depth that are less than 50 km in the Ionian basin and down to 660 km in the Tyrrhenian Basin (Engdahl et al., 1998; Selvaggi & Chiarabba, 1995).

Imaging the boundary between the downgoing slab and the upper plate along the Calabrian subduction zone is important for assessing the potential of a subduction zone to create mega-thrust earthquakes. Indeed, many authors consider that earthquake rupture cannot extend beyond the intersection with the mantle wedge, which is thought to be highly serpentinized (Byrne et al., 1988; Oleskevich et al., 1999). Other workers have hypothesized that there is a significant influx of hot mantle beneath Calabria (Westaway, 1993; Ferranti et al., 2007) and others evoke slab break-off and possible delamination beneath central E Sicily and Calabria (Piana Agostinetti et al., 2009; Faccenna et al., 2011; Giacomuzzi et al., 2012). However, the exact depth and dip of the downgoing slab, as well as the thickness and nature of the upper plate (Calabria block) remain uncertain. This study tries to unravel the slab geometry and the slab depth in the Calabrian subduction zone using wide-angle seismic data and gravity modeling as well as earthquake locations and regional tomographic data.

### 1.1 Tectonic history of the study region

The evolution of the central western Mediterranean region is driven by the convergence between the African plate and the Iberian and Eurasian plates leading to subduction initiation, slab rollback and the formation of back-arc basins (Faccenna et al., 2011; Rosenbaum et al., 2002; Handy et al., 2010; van Hinsbergen et al., 2014a; Jolivet et al., 2015) (Figure 1). NW dipping subduction and ensuing rollback is thought to have started at 35-30 Ma (Rosenbaum et al., 2002; van Hinsbergen et al., 2014a). At 25 Ma the Sardinia-Corsica block began rotating in a counter-clockwise direction in response to SE-ward retreat of the subduction (Rosenbaum et al., 2002). This led to widespread extension causing the opening of the Liguro-Provencal and Valencia basins (Séranne, 1999). The original forearc then split into individual blocks known as AlKaPeCa (Alboran, Kabylides, Peloritan, Calabria) continental terranes (Bouillin et al., 1986). The Calabrian slab rolled back to the E and the overriding continental blocks were thrust onto the margin of Adria forming the southern Apennines. The Peloritan block has overthrust the African margin of Sicily (Speranza et al., 2003). A slab length offset between the originally attached Calabrian and Kabylides slab might be at the origin of the initiation of a STEP (Subduction Transform Edge Propagator, Govers & Wortel, 2005) fault that then separated these into two slabs (van Hinsbergen et al., 2014a). The modern day forearc STEP fault is thought to be located either at the Alfeo Fault system

(Gutscher et al., 2016; 2017; Dellong et al., 2018) or at the Ionian Fault system (Polonia et al., 2011; Scarfi et al., 2018) (Figure 2). An earlier proposition that the STEP fault follows the Malta Escarpment, a 3-km high feature offshore E Sicily (Argnani and Bonazzi, 2005) formed during the Tethyan rifting history of the Ionian Sea (Gallais et al., 2011; Frizon de Lamotte et al., 2011) seems unlikely given the absence of tectonic deformation along the central to southern Malta Escarpment since the Messinian, on the basis on high-resolution seismic profiles shot across the escarpment (Gutscher et al., 2016).

### 1.2 Deep structure of the Ionian basin and the Malta escarpment

Several deep seismic reflection and refraction studies were conducted on the eastern Sicily margin in the 80's and 90's (Makris et al. 1986, Hirn et al. 1997, Nicolich et al. 2000, Catalano et al. 2001). These studies concluded that a 30 km thick continental crust underlies the Sicilian-Hyblean plateau. An Expanding Spread Profile (ESP) experiment located in the Ionian Abyssal Plain (IAP) and on the Mediterranean ridge provided the first constraints on the crustal velocities of the deep IAP, where the sedimentary cover is thinnest. The wide-angle seismic results show a 5 km thick sedimentary cover overlying a thin crust of about 7 to 9 km (de Voogd et al. 1992, Le Meur 1997). However, different interpretations were proposed including a thinned continental crust or an oceanic one. Later studies clearly imaged a 5-6 km thick oceanic crust in the basin spanning the northern IAP (Dellong et al., 2018; Dannowski et al., 2019). Previous multi-channel seismic (MCS) studies have imaged the deep structure of the Ionian Basin and the adjacent Calabrian accretionary wedge, with sediment thicknesses increasing from about 5 km (undeformed thickness) in the abyssal plain to 10-15 km within the accretionary wedge as the dip of the subducting plate below remains very shallow (1-2° on average) (Cernobori et al., 1996; Minelli and Faccenna, 2010; Polonia et al., 2011; Gallais et al., 2011; Maesano et al., 2017). An early MCS study imaged the steepening of the subducting basement as it approaches the Calabrian block (lines ION-3 and ION-4) (Cernobori et al., 1996). At the transition between the continental (Sicilian) and the deep oceanic (Ionian) domain an abrupt crustal thinning by 3km is observed along the Malta Escarpment. The escarpment was originally interpreted to be a passive margin originating from the initial opening of the Ionian Sea. Later studies proposed this to be a transform margin (Frizon de Lamotte, 2011; Gallais et al., 2011; Dellong et al., 2018, Catalano et al., 2001) which is in good agreement with an opening at the Late Triassic/Early Jurassic of the Ionian Basin (Frizon de Lamotte, 2011). Other studies propose ages ranging from Early Late Triassic (220 Ma; Speranza et al., 2012) to Late Jurassic to Early Cretaceous (Catalano et al., 2001).

Travel time tomography using local or teleseismic events has been able to image downgoing slabs in subduction zones to depth of several hundreds of kilometers (eg. Spakman et al., 1993, Spakman & Wortel, 2004, Wortel & Spakman, 2000). One of the first studies of the Italian region showed large-scale lithospheric inhomogeneity in the deep structure of the Tyrrhenian Sea (Scarpa, 1982). Positive travel-time anomalies interpreted to be a NW dipping subducting slab beneath the Calabrian arc were later imaged from teleseismic events (Amato et al., 1993). Results from 3-D teleseismic tomography focussed on the study region reveal

the downgoing slab as a fast structure extending 350 km laterally from northern Sicily to southern Campania and 400 km vertically (Cimini, 1999). A more refined mantle tomography imaged a 150-km wide slab window beneath the southern Apennines which probably opened after a slab tear occurred between the Apulian continental subduction and the Ionian oceanic slab (Chiarabba et al., 2008). These results were refined using a denser data set and led to the proposition that the subducting lithosphere remains attached along a 100-km-long segment at the central portion of the Calabrian arc (Neri et al., 2012). Global tomography models clearly image a horizontal anomaly in the transition zone at a depth of 500 km, which is interpreted to be a flat lying part of the Calabrian slab (Spakman & Wortel, 2004, Wortel & Spakman, 2000). The existence of a proposed STEP fault (Govers & Wortel, 2005, Wortel et al., 2009) was confirmed by tomographic and gravity modeling, with a proposed location of the faults in the Tindari and Crotone Basin (Neri et al., 2012, Figure 1 for location). Recent geodetic work provided evidence for toroidal flow around the retreating slab edges of the Calabrian subduction system expressed by counter-clockwise rotations at the northern and clockwise rotations at the southern edge of the slab corresponding to movements predicted by STEP faults (Palano et al., 2017). Recent tomographic studies imaged a trench-parallel slab break-off on both sides of the slab which might be still propagating, narrowing the slab. (Barreca et al., 2016; 2018; Scarfi et al., 2016; 2018). Horizontal tearing affecting both sides of the slab was proposed to result in a narrowing of the subduction system and enhanced subsidence along the still intact segment of the slab (Scarfi et al., 2018). In central Calabria the depth of the slab has been determined by source-receiver function analysis during the CAT/SCAN experiment. The results show that the slab is steeply inclined and a 4-6 km thick layer of low-velocity sediments is imaged between the oceanic crust and the continental Calabrian backstop (Piana Agostinetti et al., 2009).

Gravity anomalies at subduction zones are generally characterized by strong signatures that are linked to topographic effects, material density and temperature heterogeneities in the lithospheric mantle and the crust, or even forces and stresses induced by plate dynamics (eg. Levit and Sandwell, 1995; Krien and Fleitout, 2008 and references therein). Gravity anomaly lineaments parallel to the arc-trench axis are often observed along subduction zones. For example, a negative free-air anomaly is usually observed at the trench and above the downgoing slab, and is interpreted as a result of a topographic effect, or of the presence of a light crustal material entrapped within the subduction complex (Forte et al. 1993; Marotta et al., 2006). It was suggested that great earthquakes occur predominantly in regions with a strongly negative trench-parallel gravity anomaly (Song and Simons, 2003). Earlier studies in the Ionian sea have shown that Bouguer gravity anomalies are consistent with young subduction of an intermediate foreland lithosphere beneath two opposing subduction systems, the Apennine-Calabrian system to the SW, and the Hellenic system to the northeast (Moretti and Royden, 1988).

Determining the position of the slab at shallow depth compared to earthquake tomographic studies and using seismic and gravimetry methods remains difficult because of the thick accretionary wedge and the Messinian evaporites layers introducing velocity inversions and density anomalies. This study aims to shed light on the deep structure of the Ionian

subduction interface below the Calabro-Peloritan backstop with a higher resolution than the above mentioned tomography and receiver function studies.

### 1.3 Objectives of the study

Four wide-angle seismic profiles were acquired to provide a 3-D image of the ESicily margin and the western portion of the Calabrian subduction zone (Figures 1 and 2). Two profiles orthogonal to the E Sicily margin cross the Malta Escarpment and the transition between continental crust of the Hyblean plateau - and the Tethyan oceanic crust of the deep Ionian basin (Dellong et al., 2018). One profile close to the Medina seamounts was shot to characterize the nature of the crust below the Ionian Abyssal Plain (Dannowski et al., 2019). Our work presents the findings of the 380 km long dip line, intersecting the three other profiles, and thus provides a comprehensive 3-D structural view of the analysed sector. The dip line crosses from the undeformed domain of the Ionian Abyssal Plain, across the external (evaporitic) Calabrian accretionary complex, the internal (clastic) accretionary wedge, and all the way to the Peloritan continental domain (NE corner of Sicily), composed of Hercynian metamorphic basement currently forming the backstop of the upper plate. The objective of this combined data set is to image the complex 3-D transition between the adjacent and overlapping crustal domains, as well as the deep expression of the lateral slab tear (STEP) fault. Among the open questions which remained following the previously published work are (eg. Dellong et al., 2018): what is the geometry (depth, thickness, dip) of the downgoing oceanic crust and its relative position to the overlying backstop? How does the thickness and nature of the accreted and/or underplated sediments vary downdip? We analyze the first wide-angle seismic data compilation that can address this set of questions.

Furthermore, regional 3-D gravity modeling was performed with the aim to test end-member models for the slab depth in the Calabrian - Messina strait region. Specifically, in wide-angle profile DY-P3, the top of the subducting oceanic crust was not imaged (Dellong et al., 2018). The authors proposed two hypotheses for its position (1) significantly below the Calabrian backstop and beyond the range of the seismic rays; (2) or that the slab is part of the thick lower crustal layer of the backstop but not resolved by the OBS data given that velocity contrasts would be minor producing no high amplitude reflection. As an intervening layer with mantle velocities (first hypothesis) will produce a strong, observable gravity anomaly this problem can be resolved using 3-D gravity modeling.

## 2 Data acquisition and processing

The wide-angle seismic data were acquired in 2014 during the Dionysus survey, a collaboration between Geomar (Kiel, Germany), INGV (Rome, Italy), Ifremer and the University of Brest (both Brest, France) onboard the R/V Meteor (M111 cruise). Additionally, we used gravity data from satellite free-air anomaly from the World Gravity Map (WGM-2012 – Bonvalot et al., 2012; Pavlis et al., 2012) for gravity modeling.

### 2.1 Wide-angle seismic data

Three long and one shorter wide-angle seismic profiles were shot using an array of six GI-Guns of a total volume of 84 liters (5,440 $in^3$) (Figure 2). This work focuses on the DY-P4 profile which spans the Calabrian subduction zone along a SE-NW transect.

Half of the marine instruments used in this experiment were MicrOBS from Ifremer equipped with three-component 4.5 Hz geophones and a hydrophone both recording at a 4 ms sampling rate (Auffret et al., 2004). The other half consisted of OBH (Ocean Bottom Hydrophones) from Geomar (Bialas & Flueh, 1999). OBS were deployed on even position numbers and OBH on odd position numbers. The land stations were six REF TEK 130S-01 equipped with short period velocimeter sensors with a 1 s dominant period. Their sampling rate was set at 8 ms. The seismic source used during the survey consisted of two subarrays of 6 GI-Guns. The 12 guns together provided a volume of 84 l (5,440 $in^3$) and were operated at 190 bar. The shooting interval was set to a constant 60 s for all profiles, resulting in a shot point interval of 150 m. The marine part of the profile is co-incident with the deep reflection seismic profile CROP M2B which was used in this study to constrain the geometry of the sedimentary layers (Polonia et al., 2011) (Figures 1 and 5).

We installed 61 ocean bottom instruments along profile DY-P4 at 5-6 km intervals and 5 INGV landstations in Sicily along the prolongation of the profiles (see Figure 2). Data quality is good, however, arrivals are highly distorted and energy is lost at long offsets probably due to the highly irregular sedimentary layer boundaries and the presence of salt leading to a velocity inversion in the sedimentary column (Figures 3 and supplementary materials Figure S1). The land-station data are of very good quality and reflections picked from the data sections were one of the main inputs for the modeling of the subducting oceanic plate geometry (Figure 4). Initial processing was performed onboard, and profiles DY-P1 and DY-P3 were modelled using a forward approach (Dellong et al., 2018). This study uses an identical approach for profile DY-P4 to achieve inter-comparable models. The OBS data were corrected for time and spatial drift during the deployment on board. First arrival time picking and a preliminary tomographic inversion were equally run on board, however the resulting preliminary velocity models showed high uncertainties, due to the velocity inversion of the salt layer and the low density of seismic rays reaching lower crustal and upper mantle depth. Because of these difficulties the data were modeled using the "*Rayinvr*" software (Zelt & Smith, 1992; Zelt, 1999) to be able to include additional information from coincident reflection seismic data and gravity modeling. This approach uses a combined forward and inversion approach to model layers of different velocities and velocities gradients. Layer depth and velocities are defined by the user in the first place. A smoothed inversion at velocity and depth nodes selected by the user can be used additionally to constrain the best fitting solutions. Depending on the data quality either the hydrophone or the vertical geophone data were used for the modeling.

Travel-time picking was performed when possible on unfiltered data sections. When necessary a Butterworth frequency bandpass filter was used to enhance the signal/noise ratio. A total of 23971 picks were used for the velocity modeling, including 17 phases (Table 1).

The high number of phases is due to the lateral changes of the tectonic regime along this long profile. Although the absolute number of layers of the final velocity model is high (12 layers including water surface and Moho), the number of layers at any given position along the profile never exceeds 7. The high absolute number of layers can be explained by the lateral change of character of the sediments and crust from oceanic to the accretionary wedge and the Calabria block. Along the oceanic part of the profile, within the accretionary wedge 4 sedimentary layers were modelled using reflected and turning arrivals. The second layer is characterized by a higher velocity than the underlying one, therefore inducing a velocity inversion. At the accretionary prism 4 sedimentary layers were also picked. However, since the second and third layer show no lateral continuity to the oceanic region, two additional layers were defined to avoid confusing the readers and to demonstrate that the origin of those two layers differs from the ones to the SE. Similarly two crustal layers were picked in the oceanic domain as well as in the backstop domain resulting in 4 individual layers, which however, are not continuous along the profile.

Key reflectors in the sedimentary layers were picked from the coincident CROP M2B time section (Figure 5 this study and in more detail in Polonia et al., 2011) and included in the wide-angle seismic model to better constrain the sedimentary layer geometry. The reflectors were converted to depth with the help of the OBS data. The model was extended on land to include the landstation data, but no reverse shots exist from the land part of the profile. The OBS data constrain sedimentary, crustal and upper mantle parts of the model in the marine model. The land-station data provide constraints on the deep geometry of the necking zone. No turning wave arrivals from shallow layers on land exist as shots were only produced along the marine part of the profile (Figure 6).

### 2.2 Gravity modeling

To evaluate the impact of different scenarios for the slab depth along the DY-P3 profile, three different models were constructed differing only in the depth of the slab. The first model is the (1) *reference model*, built to closely fit the predicted free-air anomaly from the model to the measured one. Then, two end-members models were built to test a (2) *shallow slab* hypothesis (5 km shallower slab) and a (3) *deep slab* hypothesis (15 km deeper) (detailed explanations are given in supplementary Text S1).

## 3 Results

In the following section the results from the velocity modeling are presented together with their error estimation. The results from the 3-D gravity models constructed in this study are presented thereafter.

### 3.1 Seismic velocity model

The final velocity model is composed of five sedimentary units, an oceanic crustal layer subdivided into two layers (corresponding to layer 2 and 3) and a Calabrian crustal block composed of two layers (Figure 8). The deepest layer corresponds to the lithospheric mantle,

however it's velocities are only constrained by diving rays in the oceanic part. The first sedimentary layer has a velocity between 2.0 and 2.3 km/s and a variable thickness between several hundreds of meters and 2-3 km. Along model distance -30 to 140 km, the second sedimentary layer is characterized by velocities between 4.5 km/s and 4.8 km/s and with a thickness between 2 and 5 km, which is characteristic for the Messinian evaporites layer located in this part of the accretionary wedge. Towards the NW this layer thickens before being pinched out by the sedimentary units of the inner part of the accretionary wedge that has lower velocities between 2.3 km/s and 2.35 km/s and a thickness of 2-3 km. The third sedimentary layer extends from the edge of the evaporite layer towards the NW with a variable thickness of ~3 km and velocities of 2.30-2.35 km/s. It was modeled as a separate layer as the velocities change abruptly from the evaporitic layer. The fourth sedimentary layer presents a lateral velocity change with higher velocities where it is underlying the evaporites of the outer accretionary wedge (3.50 – 3.80 km/s) than in the inner accretionary wedge (2.80 – 2.90 km/s). The lowermost sedimentary layer has a velocity between 4.5 km/s to 4.8 km/s in the SE and 3.8 km/s to 4.2 km/s in the NW. Together the thickness of the sedimentary cover varies between 5 km in the SW and 18 km at 230 km model distance. The Calabro-Peloritan Block is covered by only 2-3 km of sediments. The oceanic crust is 5-6 km thick with velocities increasing from 6.5-7.2 km/s to 6.8-7.4 km/s towards the NW and has been subdivided into two distinct layers of approximately 2 and 4 km thickness. The Calabro-Peloritan block has a thickness of 30 km and was subdivided into two layers with velocities between 5.5 km/s and 6.6 km/s and diminishing to only 5.3 km/s at the tip of the backstop.

The MCS and the wide-angle seismic section show good agreement as the shallow sedimentary layers as the layer geometry was picked on the migrated time section (Polonia et al., 2011), however, MCS data offer a finer resolution of certain structures of the subduction system (i.e. thrust faults, slope basins and inverted structures in the accretionary wedge) than deep sounding wide-angle seismics (Polonia et al., 2011).

### 3.2 Error calculations

The error between the picked arrival time and the predicted time from forward modeling indicates the fit of the model to the data. The number of picks and root mean square (rms) travel-time residual for all phases are listed in Table 1. Error calculations included the calculation of the nodes uncertainty smearing into neighboring parts of the model (spread point function) (Figure S2 b), the resolution of the individual model nodes (Figure S2 d), and the number of rays passing through the different layers (ray hit count) (Figure S2 b). We also used "Vmontecarlo" software to produce a detailed analysis of the velocity uncertainties (Loureiro et al., 2016) (Figure S3). A detailed description and resulting figures are shown in the electronic supplement Text S2 and figures S2 and S3). Results from the error estimation show that the sedimentary and oceanic crustal domain are well constrained by reflected and turing rays. Here resolution is high with hit counts higher than 5000 per cell and smearing of uncertainties is be low. Resolution is lower in the Calabrian lower crustal layer with only few rays passing through the layer and underneath the salt layer due to the velocity inversion from the salt to underlying sedimentary layers. The Monte Carlo inversion shows a good fit with

uncertainties not exceeding 1.0 km/s for the deepest layers.

### 3.3 Gravity models

In the Ionian basin, the free-air anomaly increasingly positive towards the S (Figure 8). The Apulian and Malta escarpments are characterized by strong positive free-air anomalies. In central Sicily a negative anomaly contrasts with the positive free-air anomaly of Mount Etna, the Peloritan Mountains and the Hyblean Plateau. In the Tyrrhenian basin a relatively homogeneous anomaly is observed with a value of approximately 50 mGal with the exception of the Eolian Islands presenting stronger anomalies.

The 3-D gravity models were built to reproduce these main features observed in the free-air anomaly. The long wavelength features of the free-air anomaly data are well reproduced throughout the three 3D gravity models, showing that the deep density variations are explained by our models. Short wavelength variation are less well reproduced, meaning that some shallower features maybe missing in the models.

The *reference model* places the top of the oceanic crust at a depth of about 30 km along this profile comparable to the wide-angle seismic model. For the "*deep slab*" model, the top of the oceanic crust is set at a depth of about 45 km along the A2B2 cross-section. The slab then deepens to 60 km to the N-E along the GH cross-section allowing to observe the 3-D effect of a high-density body sandwiched in between the Calabrian continental crust and the oceanic crust. The calculated anomaly from this *deep slab* model increases by about 20 mGal with respect to the *reference model* and also affects the resulting anomaly beyond the direct slab depth deepening zone, in an area greater than 30 km. To the N, along the GH cross-section, the slab deepening resulted in an increase of 10 mGal in the calculated anomaly in comparison to the reference model and in the S, along the ST cross-section, in an increase of less than 5 mGal.

For the "shallow slab" model, the oceanic crustal layer depth was decreased to 20-25 km along the A2B2 cross-section. This configuration is a more realistic hypothesis suggested in the past (Dellong et al., 2018). This model resulted also in an increase of the calculated gravity anomaly with respect to the reference model. But this increase is significantly greater than the one calculated for the "deep slab" model, and is about 30 mGal. This modification does not affect the gravity anomaly at a large wavelength as this increase is only calculated for the areas that are close to the modification (less than 10 km along the cross-section). To the N (along the GH cross-section) we observed a small effect of this modification on the gravity anomaly (less than 5 mGal). However, it is characterized by a decrease of the anomaly in comparison to the reference model. In addition, to the S, along the ST cross-section this shallow slab model shows an increase of less than 5 mGal of the calculated gravity anomaly.

Three mantle densities were used to satisfactorily fit the data. These reflect three different geodynamical origins: a continental Hyblean mantle layer derived from the wide-angle velocity models (at 3.33 g/cm$^3$ shown in red in Figure 8 in more detail in supplementary material Figure S4 and Table S1); an oceanic mantle layer (3.35 g/cm$^3$, in blue), and a back-arc mantle layer (3.22 g/cm$^3$, in pink). The relative difference of these values depends on the depth of the gravity model. However from preliminary tests it is clear that models using one single density for the mantle do not allow to sufficiently fit the data. These last two layers were obtained by extrapolating the tomographic models (Scarfi et al., 2018) and therefore do not have a corresponding velocity in Table S1, which provides only velocities from wide-angle seismic modeling. The difference between the Hyblean and Tethyan oceanic mantle domains is small and can be explained by several factors, such as mantle composition or thermal state. However, the density of the Tyrrhenian mantle is significantly different as also observed in the tomographic model (Scarfi et al., 2018). This difference is probably related to the post-Messinian back-arc extension, subduction induced mantle convection, ensuing asthenospheric upwelling and associated very high heat flow (Zito et al., 2003).

2D gravity models produced using the "xgravmod" software of Colin Zelt along the profile DY04 are shown in the electronic supplements (Zelt, 1999; supplementary Text S3 and Figure S5). In this more detailed model densities from the seismic velocities the sedimentary and oceanic crustal sections and the mantle velocities from the 3D gravity modeling were taken into account. The resulting fit is high and allows to reproduce small gravity anomalies unresolved by the 3D models.

## 4 Discussion

### 4.1 Gravity

The results obtained from the three 3-D gravity models, show that the reference model has the best fit to the free air gravity anomaly. In this reference model the top oceanic crust is located at around 25 to 30 km depth along the A2B2 cross-section (specifically along the DY-P3 velocity model). Based on the hypothesis that the recorded seismicity is predominantly intra-crustal, the corresponding slab depth is in good agreement with either the reference model and/or the shallow slab model along the DYP3 profile. The three gravity models allow us to conclude that a mantle wedge is highly unlikely to exist below the Calabrian backstop along the DY-P3 velocity profile. The models show relatively large uncertainties concerning the depth of the interfaces of ±2.5 km for the Moho interface and the top of the oceanic crust. These results are in agreement with the DY-P4 velocity model and also the tomographic model from Scarfi et al., 2018. Three different lithospheric mantle densities enabled us to reproduce the large-scale regional observed free-air gravity anomaly and then test the three slab depth hypotheses. These densities were attributed to the Tethyan oceanic domain (3.35 g/cm$^3$), the mantle below the Hyblean plateau (3.33 g/cm$^3$) and the mantle of the Tyrrhenian backarc domain (3.22 g/cm$^3$), respectively. The difference between the Hyblean and Tethyan mantle domains is fairly small and can be explained by several factors, such as composition or thermal state of the mantle. However, the density of the Tyrrhenian mantle is significantly different as also observed in the tomographic model (Scarfi et al., 2018). This difference is

probably related to the post-Messinian back-arc extension, asthenospheric upwelling and associated very high heat flow (Zito et al., 2003).

### 4.2 Velocity models

A comparison of the DY-P4 velocity model with the three previously published velocity models (DY-P1, DY-P3 and DY-P5) (Dellong et al., 2018; Dannowski et al., 2019) provides a 3-D view of the Ionian basin (Figure 9). The fit at the crossing points is good, with slight differences that may be due to anisotropy or data quality (Figure 7 d,e,f). Sedimentary thickness in the basin is highest at the backstop contact (10-12 km). The Messinian salt layer is imaged along profiles DY-P1 , DY-P4 and DY-P5 with a thickness of up to 4 km. A layer of high velocity sediments is imaged in the southern part of the basin (4.5 – 4.8 km/s). This high P-wave velocity layer, showing parallel high amplitude reflections has long been described below the IAP (Makris et al., 1986; de Voogd et al., 1992; Minelli & Faccenna, 2010; Gallais et al., 2011) and likely represents Jurassic deep water carbonates, the only sedimentary rocks with such high velocities aside from halite (Anselmetti and Eberli, 1993). Oceanic crust underlying the basin is ~5 km thick, implying it is thinner than normal Atlantic ocean crust from existing compilations throughout the basin, which has a mean thickness of 7.1 km (White et al., 1992). Crustal thickness increases abruptly at the Malta escarpment (DY-P1), and at the Sicily Margin (DY-P3) and the Peloritan backstop (DY-P4), indicating the presence of continental crust in these domains (Figure 9). Similarly, in both DY-P3 and DY-P4 velocity models, the upper crustal velocities increase laterally toward the continental blocks of the Sicily margin (DY-P3, from 5.0 to 6.0 km/s) and Peloritan backstop (DY-P4, from 4.75 to 5.75 km/s). These two continental domains differ in their lower crustal layers with higher velocities in the Sicily margin. While the DY-P1 and DY-P3 are imaging the same continental Sicily margin through the Malta Escarpment, profile DY-P4 images a different continental block that is likely related to Peloritan backstop, inherited from the roll-back of the Calabrian Subduction. Another discrepancy between DY-P3 and DY-P4 is the presence of the slab (Figure 7 and supplementary material Figure S6). While along DY-P3 no slab was modeled, along the profile DY-P4 the slab is clearly imaged by the data from the land-stations. This difference is due to the fact that the data quality of the land-stations along DY-P4 is very high, and from OBS data alone on DY-P3 the slab could not be detected. Furthermore, the ENS-WSW orientation of profile DY-P3 very close to and parallel to the NW dipping slab hinge was unfavorable for recording deep crustal or upper mantle arrivals, as most of the seismic energy from the airgun shots would be transmitted down dip to the NW and off profile. The Moho depth along model distance 80-120 km on profile DY-P3 (31 km) corresponds to the depth of the oceanic Moho along DY-P4, however, the backstop-slab interface was not detected along DY-P3 (Figure 9). This result is in good agreement with results from the gravity modeling. In the S DY-P4 intersects with profile DY-P5 where both profiles image thin crust interpreted to be of oceanic origin (Dannowski et al., 2019).

Comparison of these results with existing compilations of crustal thickness and Moho depth shows a good agreement in the center of the basin (Nicolich et al., 2000), but significant differences exist at the Sicily margin and the Malta escarpment, where the older studies

propose relatively thin crust (~24 km) compared to our data that suggest a thickness of up to 30 km. These differences are probably due to the paucity earlier, wide-angle seismic data along these margins.

During the CAT/SCAN seismic experiment 18 land-stations were deployed to record teleseismic events during nearly 2 years at the Sila Plateau in southern Italy. Using receiver functions from 586 events the depth of the Ionian Moho was calculated to lie at around 35 km underneath the eastern part of Calabria gently dipping westward (Piana Agostinetti et al., 2009). The depth increases steeply to ~80 km beneath western Calabria. This study is located about 150 km N of DY-P4 so direct comparisons are not possible. However, the thickness of the Calabrian crust and steep dip of the subducting crust are in good agreement with our results. The authors also propose the existence of a 6-10 km thick layer of underplated sediments between the Ionian and Calabrian crust, which was not imaged in our velocity model. This might be due to the fact that our velocity model in the NW end is mainly constrained by reflected arrivals from the land stations, which might render the detection of low velocity zones difficult. Also this observation is based on S-wave velocities, which we were not able to model. Another explanation might be that our profile is located at the western edge of the subduction zone, where the crust is located at a shallower depth with respect to the center of the arc as imaged by tomography (Maesano et al., 2017, Scarfi et al., 2018). In central Calabria, the slab is highly arcuate and may transport a greater amount of sediments.

### 4.3 Results from earthquake tomography

A detailed tomographic image of the Calabrian subduction was constructed from local earthquakes (Scarfi et al., 2018) (Figure 10). The results indicate that the slab is continuous only below the southern Calabro-Peloritan arc where its curvature is highest. In the SW, deformation at the free slab edge has led to detachment of a slab fragment and the formation of a slab window between 50 and 100 km (Scarfi et al., 2018). Comparing the wide-angle seismic velocity model, with results from the earthquake tomography and earthquake distribution, allow us to correlate the shallow layers to the deep mantle structures. The downgoing slab is continuous and steeply inclined in this region and can be traced as a high P-wave velocity anomaly as well as by using the distribution of earthquake hypocenters. The Moho depths are similar in the Ionian Basin, and in the part of the arc constrained by seismic rays. The thickness of the low velocity accretionary wedge is similar as well. The tomographic model shows that the physical properties of the mantle differ between the Ionian and the Tyrrhenian Basins, which led us to use different values for our gravity modeling. The low velocity anomaly in S-wave velocity indicated from receiver function analysis (Piana Agostinetti et al., 2009) does not correspond to a low velocity zone in P-wave velocity in the tomographic model.

Particularly interesting features of the Calabrian slab geometry as constrained by our wide-angle seismic data and the tomographic image are: the extremely shallow average dip of 1.3° of the subducting oceanic crust over the frontal 200 km, (deepening from 11 km to about 16

km), the slab hinge where the slab dip increases abruptly from 2-5° to 60-70° over a distance of ≤50 km. By comparison with regional tomography data, only the very steep dip of the deep slab below 60 km depth (about 70°) can be deduced. One of the novelties of this work is the first successful imaging using wide-angle seismic data of a slab hinge with such an extremely abrupt steepening.

Finally, the very narrow geometry of the Calabrian slab (lateral width ≤200 km) (Neri et al., 2012; Scarfi et al., 2018) may contribute to the steep dip. Indeed, numerous analogue (Funiciello et al., 2006; Schellart, 2004) and numerical modeling studies (Govers & Wortel, 2005) have shown that for narrow slabs, the toroidal flow around the slab is facilitated, enabling the slab to roll back more rapidly and contributing to increasing its dip (see also section 4.4 below on deep slab geometries). SKS splitting observed in the mantle below southern Italy confirm strong toroidal flow behind the Calabrian slab (Civello & Margheriti, 2004). Such extremely narrow slabs (e.g. - Calabria, Gibraltar) were excluded in the global analysis of subduction zones since their segment lengths were considered too short to be representative of typical slab behavior free of edge effects (Heuret et al., 2006, Lallemand et al., 2005).

### 4.4 Narrow curved subduction zones and deep slab structure

Global travel time tomographic images of the upper mantle reveal slab geometries at large scale (Bijwaard et al., 1998) and can also image ongoing geodynamic processes such as slab tearing and slab detachment (Wortel and Spakman, 2000). Here we present three examples of deep slab geometries, two from narrow curved arcs (Gibraltar and Calabria) and one from a much longer laterally continuous subduction zone (Northern Honshu), unsegmented over nearly 1000 km (Figure 11). The Calabrian subduction and Gibraltar subduction are possibly the narrowest arcs in the world, with lateral widths of ≤300km and ≤200km, respectively (Wortel and Spakman, 2000; Gutscher et al., 2002; Faccenna et al., 2004; Gutscher et al., 2017). In both cases wide-angle seismic studies have concluded that the downgoing lithosphere is most likely oceanic in nature and of Jurassic age (Sallares et al., 2010; Dellong et al., 2018). Both subduction systems are characterized by extremely wide (~200km down-dip direction) accretionary wedge complexes, with very shallow surface angles and thus narrow tapers (Gutscher et al., 2002; 2009; 2012; Gallais et al., 2012; Gutscher et al., 2017; Dellong et al., 2018). There is a broad consensus that apart from their large-scale morpho-tectonic similarities, that both subductions formed through roll-back of narrow slabs over the past 5 - 10 million years (Gutscher et al., 2002; Faccenna et al., 2004; Chertova et al., 2014; van Hinsbergen et al., 2014b; Gutscher et al., 2017; Palano et al., 2017). The overall slab geometry of both systems is also largely similar. As discussed above, the dip of the downgloing plate is very shallow below the accretionary wedge (typically 1-5°). The plate dip increases abruptly below the overriding continental fore-arc block to 30 - 45° where the slab reaches depths of 50 - 100 km (Figure 11 a,b). Below 100 km (for Calabria) and below 150 km depth (for Gibraltar) the slab dip increases to >60°, locally approaching a sub-vertical geometry (Figure 11 a,b). There are also deeper sub-horizontal high p-wave velocity anomalies between 600 km and 660 km depth, below the Betics (S Spain) and below Corsica

- Sardinia, related to the older portions of the Gibraltar and Calabrian subductions, respectively and already discussed at length by previous authors (Wortel and Spakman, 2000; Faccenna et al., 2004; Bezada et al., 2013; Chertova et al., 2014; van Hinsbergen et al., 2014b) and which are consistent with the long-term slab roll-back kinematics which have resulted in these narrow arcs. More recent detailed tomographic work using earthquake travel time data from local seismic networks have imaged the lateral slab tears and nearby portions of detached slabs and conclude that these two sytstems are approaching the terminal stages of subduction (Bezada et al., 2013; Neri et al., 2009; Scarfi et al., 2018).

There are some differences between the tomographic images from the respective back-arc domains, however. The Calabrian back-arc (below the Tyrrhenian Sea) shows a broader stronger low p-wave velocity anomaly, than the corresponding back-arc domain from the Gibraltar subduction (below the Alboran Sea), which exhibits a thinner zone of higher temperature asthenosphere at shallower depths (50-150 km) and further in the back-arc presents a less pronounced and more heterogeneous anomaly (Figure 11 c,d). While the estimated modern day subduction velocities are very small for both subduction systems, for Calabria 3 - 5mm/yr (Palano et al., 2012; 2017), and ~5mm/yr for Gibraltar, (Koulali et al., 2011; Palano et al., 2015), it is thought that the Tyrrhenian Sea back-arc basin had two major phases of opening linked to rapid slab roll-back, inducing vigorous mantle convection (Faccenna et al., 2001). Furthermore, the larger Tyrrhenian Sea back-arc basin, evolved all the way to seafloor spreading (Marani and Trua, 2002), whereas the W Alboran basin, while highly extended, never reached seafloor spreading (Watts et al., 1993; Booth-Rea et al., 2007; Medaouri et al., 2014). A broader subducting segment (300km vs 200km), and a larger, fully developed back-arc basin both imply more vigorous convection in the asthenospheric wedge above the subducting Calabrian slab (Figure 11 a,b).

The N Honshu subduction (NE Japan Trench) has a very different overall slab geometry with a nearly constant shallow (50 - 150 km depth) and deeper (200 - 500 km depth) slab dip of about 30 – 35° (Figure 11 e,f). The age of the subducting lithosphere is Mesozoic, about 130 Ma (Mueller et al., 1997) and therefore rather similar to the estimated age of the lithosphere subducting below Calabria or Gibraltar. It should be noted, however, that in fact there is no statistically significant correlation between the age of the subducting lithosphere and the slab dip based on a global analysis of subduction zone parameters (Lallemand et al., 2005). Other factors play a more dominant role like the nature of the upper plate (continental vs. oceanic) or the overall kinematics of the fore-arc and back-arc (extension vs. convergence) (Lallemand et al., 2005). The reasons for the constant and very modest slab dip below N Japan and extending below NE China are probably related to an anchoring of the Pacific slab at the 660 discontinuity below NE China and a stationary trench (in a Eurasia fixed reference frame) and to the large lateral width (1000 km) of the unsegmented Pacific slab, before changing its orientation at the Kurile trench. A long, laterally continuous slab favors poloidal flow, while limiting toroidal flow around the lateral slab edge and creates a very stable kinematic configuration for the large-scale slab (Schellart, 2004; Lallemand et al., 2005). Finally, there are also major differences in the overall level of seismicity in the three slabs (Figure 11 e,f). While the N Honshu slab is marked by abundant seismicity down to 200 km and then

scattered seismicity down to 500 km (Figure 11 c), the Calabrian slab is also marked by abundant intermediate depth seismicity down to 300 km and thereafter less abundant but still clearly marked seismicity down to 500 km (Figure 11 a). In contrast, the Gibraltar slab exhibits a cluster of intermediate depth seismicity between 60 km and 120 km depth and no deeper seismicity below (Buforn et al., 2004) (Figure 11 b). It has been suggested that this is evidence for a horizontal tear (slab detachment) occurring here (Heit et al., 2017), though an alternative explanation is the presence of extreme bending stresses as the slab abruptly steepens (Gutscher et al., 2002). Deep focus earthquakes occur below Granada (S Spain) (Buforn et al., 2011) and confirm the presence of a deep slab here interacting with the 660km discontinuity (Bezada et al., 2013).

### 4.5 Comparison of two thick accretionary wedges with thick incoming sedimentary sections

If we compare the accretionary wedges from Sumatra and Calabria (Figure 12), the cross-sectional areas of the two accretionary wedges are quite similar. For Calabria the wedge is about 250 km wide (down-dip width) with a maximum thickness of 12-13 km and an incoming sedimentary thickness of 5-6 km. For Sumatra, the incoming sedimentary thickness is identical (5 km) and the width of 150 km and maximum thickness of 20 km are 40% less and 50% more than for Calabria, respectively. The main differences are the surface slope angles which are much lower for Calabria (~1°) than for Sumatra (2-3° with an overall convex shape) and the dip of the downgoing plate. For Calabria as discussed above it is a regular, constant 1.3° dip over 200 km and then the dip steepens sharply (Figure 12). For Sumatra the dip is about 3° below the deformation front, and it increases progressively to 10° at 20 km depth (contact with the upperplate backstop at profile km 200). The dip remains roughly 10° down to 40 km depth (Figure 12 A). The overall geometry of the Sumatra subduction resembles an ideally bulged lithosphere, with a marked 1 km high flexural bulge visible in the wide angle seismic data (Figure 12 A, model km 50) but buried beneath the thick Bengal Fan sediments. There would be a deep sea trench, characteristic of most subduction zones, were it not for the enormous quantity of sediments (5 km) drowning this morphological feature. The Calabrian subduction does not show this broad scale flexure and has no flexural bulge. This may be in part due to the fact that it is a very narrow slab and that our seismic profile is sampling the edge of the subduction zone or due to the stiffness of the plate. In the SE and central part of the profile (Figures 11 and 12, model km 0 - 200), the oceanic crust is still attached to the W to the continental crust of the Hyblean domain. The slab dip increases abruptly NW of the termination of the lateral slab tear fault (model km 280 – 300).

A second observation from this comparison is that the accretionary wedge in the Ionian Basin is characterised by a very shallow slope in comparison to other subduction zones with thick accretionary wedges. This fact is possibly related to the presence of Messinian evaporites in a large part of the wedge which will facilitate sediment sliding gradually down the slopes (Minelli & Facenna, 2010) and therefore facilitate the buildup of a large accretionary prism. The very low taper angle of the external Calabrian Arc accretionary wedge is comparable to

that proposed for the neighbouring salt bearing Mediterranean Ridge by Kastens (1991) through analysis of sediment facies within the wedge. Low slope angles might be explained by the mechanical strength of the evaporites over a very weak basal detachment that favours outward growth rather than vertical stacking of accreted units (Polonia et al., 2011). The composition of sediments along the subducting plate and in the accretionary prism have a direct influence on the hydrogeology, fluid budgets and geotechnical properties of the plate-boundary (Underwood, 2007). Sediment thickness and the lithostratigraphy of the incoming plate influence the physical properties of the margin inducing lateral heterogeneities in the prism formation (Ike et al., 2008). Also, salt layers influence the tectonic deformation style and spatial variation in pore water salinity resulting in differences in fluid density and can therefore drive large scale fluid and heat transport (Sarkar et al., 1995) impacting on the position of the updip limit of the seismogenic zone.

## 5 Conclusions

From gravity modeling we conclude that along the DY-P3 profile, the gravity model with the oceanic slab at an intermediate depth of about 25 km shows the best fit. This model implies that there is no mantle layer between the Calabrian backstop crust and the dipping slab. In order to obtain a good fit to the observed gravity anomaly and with respect to the tomographic models, the mantle densities in the Tethyan oceanic domain (3.35 g/cm$^3$) must differ substantially from those in the Tyrrhenian backarc domain (3.22 g/cm$^3$). This is in good agreement with the fact that the basins are of different ages and with the presence of hot, convecting mantle/asthenosphere beneath the back-arc domain.

The velocity model for the DY-P4 profile images thin oceanic crust throughout the basin beneath the accretionary prism. At the NW end of the profile the Calabrian backstop extends underneath the accretionary wedge to about 100 km SE of the Calabrian coasts. The thick accretionary wedge is divided in four layers comprising a high velocity evaporitic layer and a high velocity stratified layer deposited directly on top of the oceanic basement and probably consisting of deep-water carbonates. The presence of Messinian evaporites in a large part of the wedge causing a very low basal friction facilitates lateral spreading during convergence and favors construction of a very long, shallowly tapered accretionary prism.

Prolongation of the model using earthquake hypocenters and regional tomographic data indicates that the slab dip increases abruptly from 2-3° to 60-70° over a distance of ≤50 km underneath the Calabrian backstop. This might be related to the roll-back geodynamic evolution of the narrow Calabrian slab which is similar to the Gibraltar slab showing a very comparable geometry.

## Acknowledgements

We thank the captain and crew of the R/V Meteor for the data acquisition during the marine survey. The DIONYSUS cruise (M111) was funded through the Deutsche Forschungsgemeinschaft DFG. We also acknowledge Région Bretagne and Ifremer for funding the PhD scholarship associated to this work, as well as the University of Western

Brittany (UBO) and the LabexMer for their help and funding of this work. We would like to acknowledge scientists and technical teams of the INGV for deploying the land-stations and Bruno Marsset from Ifremer for help processing these data. Most of the figures from this paper were generated using the Generic Mapping Tools (http://gmt.soest.hawaii.edu) and the Seismic Unix software was used for processing the wide-angle seismic data (https://github.com/JohnWStockwellJr/SeisUnix/wiki) (Cohen and Stockwell, 2003). The free OpendTect from dGB Earth Sciences (https://www.dgbes.com/index.php/download) and the open source Qgis software (https://www.qgis.org/fr/site/forusers/download.html) were used for data processing and drafting of several figures. The ocean-bottom seismometer data used in this publication are accessible in standard Segy format upon request at http://doi.org/10.17882/52435

**References**

Amaru, M. L. (2007). *Global travel time tomography with 3-D reference models* (Vol. 274). Utrecht University.

Amato, A., Alessandrini, B., Cimini, G., Frepoli, A., & Selvaggi, G. (1993). Active and remnant subducted slabs beneath Italy: evidence from seismic tomography and seismicity. *Annals of Geophysics*, *36*(2).

Anselmetti, F.S., and Eberli, G.B., (1993). Controls on sonic velocity in carbonates. Pure Appl. Geophys., 141, 287-323.

Argnani, A., and Bonazzi, C., (2005), Malta Escarpment fault zone offshore eastern Sicily: Plio-Quaternary tectonic evolution based on new multi-channel seismic data: Tectonics, v. 24, TC4009, doi:10.1029/2004TC001656.

Auffret, Y., Pelleau, P., Klingelhoefer, F., Geli, L., Crozon, J., Lin, J. Y., & Sibuet, J. C. (2004). MicrOBS: A new generation of ocean bottom seismometer. *First Break*, *22*(7), 41-47.

Barreca, G., Scarfì, L., Cannavo, F., Koulakov, I., & Monaco, C. (2016). New structural and seismological evidence and interpretation of a lithospheric-scale shear zone at the southern edge of the Ionian subduction system (central-eastern Sicily, Italy). Tectonics, 35, 1489–1505. doi:10.1002/2015TC004057.

Barreca, G., Branca, S., & Monaco, C. (2018). Three-Dimensional Modeling of Mount Etna Volcano: Volume Assessment, Trend of Eruption Rates, and Geodynamic Significance. *Tectonics*, *37*(3), 842-857.

Bezada, M. J., E. D. Humphreys, D. R. Toomey, M. Harnafi, J. M. Davila, and J. Gallart (2013). Evidence for slab rollback in westernmost Mediterranean from improved upper mantle imaging, Spain, *Earth Planet. Sci. Lett.*, 368, 51–60, doi:10.1016/j.epsl.2013.02.024.

Bialas, J., & Flueh, E. R. (1999). Ocean bottom seismometers. *Sea Technol*, *40*(4), 41-46.

Bijwaard, H., Spakman, W. and Engdahl, E.R. (1998). Closing the gap between regional and global travel time tomography. *Journal of Geophysical Research* 103, 30,055-30,078.

Bonvalot, S., Balmino, G., Briais, A., Kuhn, M., Peyrefitte, A., Vales, N., ... & Reinquin, F. (2012). World gravity map. *Bureau Gravimetrique International (BGI), Map, CGMW-*

*BGI-CNES728, IRD, Paris*.

Booth-Rea, G., Ranero, C.R., Martínez-Martínez, J.M., and Grevemeyer, I. (2007). Crustal types and tertiary tectonic evolution of the Alboran sea, western Mediterranean. *Geochemistry, Geophysics, Geosystems* , v.8, doi:10.1029/2007GC001639.

Bouillin, J. P., Durand-Delga, M., & Olivier, P. (1986). Betic-Rifian and Tyrrhenian arcs: distinctive features, genesis and development stages. In *Developments in Geotectonics* (Vol. 21, pp. 281-304). Elsevier.

Brocher, T. M. (2005). Empirical relations between elastic wavespeeds and density in the Earth's crust. *Bulletin of the seismological Society of America*, *95*(6), 2081-2092.

Buforn, E., M. Bezzeghoud, A. Udías, and C. Pro (2004). Seismic sources of the Iberia-African plate boundary, *Pure Appl. Geophys.* 161, 623–646.

Buforn, E., C. Pro, S. Cesca, A. Udías, and C. del Fresno (2011), The 2010 Granada, Spain, Deep Earthquake. *Bull. Seism. Soc. Am*., 101, 5, 2418–2430. doi: 10.1785/0120110022.

Byrne, D. E., Davis, D. M., & Sykes, L. R. (1988). Loci and maximum size of thrust earthquakes and the mechanics of the shallow region of subduction zones. *Tectonics*, *7*(4), 833-857.

Carminati, E., Negredo, A. M., Valera, J. L., & Doglioni, C. (2005). Subduction-related intermediate-depth and deep seismicity in Italy: insights from thermal and rheological modeling. *Physics of the earth and planetary interiors*, *149*(1-2), 65-79.

Casalbore, D., Ridente, D., Bosman, A., & Chiocci, F. L. (2017). Depositional and erosional bedforms in Late Pleistocene-Holocene pro-delta deposits of the Gulf of Patti (southern Tyrrhenian margin, Italy). *Marine Geology*, *385*, 216-227.

Catalano, R., Doglioni, C., & Merlini, S. (2001). On the mesozoic Ionian basin. *Geophysical Journal International*, *144*(1), 49-64.

Cernobori, L., A. Hirn, J.H. McBride, R. Nicolich, L. Petronio, M. Romanelli, and STREAMERS/PROFILES Working Groups, 1996. Crustal image of the Ionian basin and its Calabrian margins, *Tectonophys*., 264, 175-189.

Chertova, M. V., W. Spakman, T. Geenen, A. P. van den Berg, and D. J. J. van Hinsbergen, (2014). Underpinning tectonic reconstructions of the western Mediterranean region with dynamic slab evolution from 3-D numerical modeling, *J. Geophys. Res.* (Solid Earth), 119, 5876–5902, doi:10.1002/2014JB011150.

Chiarabba, C., De Gori, P., & Speranza, F. (2008). The southern Tyrrhenian subduction zone: deep geometry, magmatism and Plio-Pleistocene evolution. *Earth and Planetary Science Letters*, *268*(3-4), 408-423.

Christensen, N. I., & Mooney, W. D. (1995). Seismic velocity structure and composition of the continental crust: A global view. *Journal of Geophysical Research: Solid Earth*, *100*(B6), 9761-9788.

Cimini, G. B. (1999). P-wave deep velocity structure of the Southern Tyrrhenian Subduction Zone from nonlinear teleseismic traveltime tomography. *Geophysical Research Letters*, *26*(24), 3709-3712.

Civello, S., and L. Margheriti (2004), Toroidal mantle flow around the Calabrian slab (Italy) from SKS splitting, Geophys. Res. Lett., 31, L10601, doi:10.1029/2004GL019607

Cohen, J. K., & Stockwell Jr, J. W. (2000). CWP/SU: Seismic Unix Release 35: a free package for seismic research and processing. *Centre for Wave Phenomenon, Colorado*

*School of Mines*.

Dannowski, A., Kopp, H., Klingelhoefer, F., Klaeschen, D., Gutscher, M. A., Krabbenhoeft, A., Klaucke, I. (2019). Ionian Abyssal Plain: a window into the Tethys oceanic lithosphere. *Solid Earth*, *10*(2), 447-462.

Dellong, D., Klingelhoefer, F., Kopp, H., Graindorge, D., Margheriti, L., Moretti, M., ... & Gutscher, M. A. (2018). Crustal Structure of the Ionian Basin and Eastern Sicily Margin: Results From a Wide-Angle Seismic Survey. *Journal of Geophysical Research: Solid Earth*, *123*(3), 2090-2114.

de Voogd, B., Truffert, C., Chamot-Rooke, N., Huchon, P., Lallemant, S., & Le Pichon, X. (1992). Two-ship deep seismic soundings in the basins of the Eastern Mediterranean Sea (Pasiphae cruise). *Geophysical Journal International*, *109*(3), 536-552.

Engdahl, E. R., van der Hilst, R., & Buland, R. (1998). Global teleseismic earthquake relocation with improved travel times and procedures for depth determination. *Bulletin of the Seismological Society of America*, *88*(3), 722-743.

Faccenna, C., F. Funiciello, D. Giardini, and P. Lucente (2001). Episodic back-arc extension during restricted mantle convection in the central Mediterranean, *Earth Planet. Sci. Lett.*, 187, 1 - 2, 105 -116.

Faccenna, C., Piromallo, C., Crespo-Blanc, A., Jolivet, L., & Rossetti, F. (2004). Lateral slab deformation and the origin of the western Mediterranean arcs. Tectonics, 23(1).

Faccenna, C., P. Molin, B. Orecchio, V. Olivetti, O. Bellier, F. Funiciello, L. Minelli, C. Piromallo, and A. Billi (2011). Topography of the Calabria subduction zone (southern Italy): Clues for the origin of Mt. Etna, Tectonics, 30, TC1003, doi:10.1029/2010TC002694.

Ferranti, L., Monaco, C., Antonioli, F., Maschio, L., Kershaw, S., & Verrubbi, V. (2007). The contribution of regional uplift and coseismic slip to the vertical crustal motion in the Messina Straits, Southern Italy: evidence from raised Late Holocene shorelines. *Journal of Geophysical Research: Solid Earth*, *112*(B6).

Forte, A. M., Dziewonski, A. M., & Woodward, R. L. (1993). Aspherical structure of the mantle, tectonic plate motions, nonhydrostatic geoid, and topography of the core-mantle boundary. *GEOPHYSICAL MONOGRAPH-AMERICAN GEOPHYSICAL UNION*, *72*, 135-135.

Frizon de Lamotte, D., Raulin, C., Mouchot, N., Wrobel-Daveau, J. C., Blanpied, C., & Ringenbach, J. C. (2011). The southernmost margin of the Tethys realm during the Mesozoic and Cenozoic: Initial geometry and timing of the inversion processes. *Tectonics*, *30*(3).

Funiciello, F., M. Moroni, C. Piromallo, C. Faccenna, A. Cenedese, and H. A. Bui (2006), Mapping mantle flow during retreating subduction: Laboratory models analyzed by feature tracking, J. Geophys. Res., 111, B03402, doi:10.1029/2005JB003792.

Gallais, F., Gutscher, M. A., Graindorge, D., Chamot-Rooke, N., & Klaeschen, D. (2011). A Miocene tectonic inversion in the Ionian Sea (central Mediterranean): Evidence from multichannel seismic data. *Journal of Geophysical Research: Solid Earth*, *116*(B12).

Gallais, F., Gutscher, M.-A., Klaeschen, D., and Graindorge, D. (2012). Two-stage growth of the Calabrian accretionary wedge in the Ionian Sea (Central Mediterranean): Constraints from depth migrated multi-channel seismic data. *Marine Geology*, v. 326-

328, p. 28-45, doi: 10.1016/j.margeo.2012.08.006.

Giacomuzzi, G., Civalleri, M., De Gori, P., & Chiarabba, C. (2012). A 3D Vs model of the upper mantle beneath Italy: Insight on the geodynamics of central Mediterranean. *Earth and Planetary Science Letters*, *335*, 105-120.

Govers, R., & Wortel, M. J. R. (2005). Lithosphere tearing at STEP faults: Response to edges of subduction zones. *Earth and Planetary Science Letters*, *236*(1-2), 505-523.

Gutscher, M.-A., Malod, J., Rehault, J.-P., Contrucci, I., Klingelhoefer, F., Mendes-Victor, L., and Spakman, W. (2002). Evidence for active subduction beneath Gibraltar. *Geology*, v. 30, p. 1071-1074.

Gutscher, M.-A., Roger, J., Baptista, M.A., Miranda, J.M., and Tinti, S. (2006). The source of the 1693 Catania earthquake and tsunami (Southern Italy): New evidence from tsunami modeling of a locked subduction fault plane. Geophysical Research Letters, v. 33, n.8, L08309 10.1029/2005GL025442.

Gutscher, M.-A., Dominguez, S., Westbrook, G.K., Gente, P., Babonneau, N., Mulder, T., Gonthier, E., Bartolome, R., Luis, J, Rosas, F., Terrinha, P., and the Delila and DelSis Scientific Teams (2009). Tectonic shortening and gravitational spreading in the Gulf of Cadiz accretionary wedge: observations from multi-beam bathymetry and seismic profiling. Sp. Vol. on Submarine instabilities, *Marine and Petroleum Geology*, v. 26, p. 647-659, doi:10.1016/j.marpetgeo. 2007.11.008.

Gutscher, M.-A., Dominguez, S., Westbrook, G., Le Roy, P., Rosas, F.M., Duarte, J.C., Terrinha, P., Miranda, J.M., Gailler, A., Sallares, V., and Bartolome, R. (2012). The Gibraltar subduction: A decade of new geophysical data. Tectonophysics v. 574-575, p. 72-91, doi: 10.1016/j.tecto.2012.08.038.

Gutscher, M.-A., Dominguez, S., Mercier de Lepinay, B., Pinheiro, L., Gallais, F., Babonneau, N., Cattaneo, A., LeFaou, Y., Barreca, G., Micallef, A., and Rovere, M., (2016). Tectonic expression of an active slab tear from high-resolution seismic and bathymetric data offshore Sicily (Ionian Sea). Tectonics, v. 35, n.1, doi:10.1002/2015TC003898.

Gutscher, M.-A., Kopp, H., Krastel, S., Bohrmann, G., Garlan, T., Zaragosi, S., Klaucke, I., Wintersteller, P., Loubrieu, B., Le Faou, Y., San Pedro, L., Dominguez, S., Rovere, M., Mercier de Lepinay, B., Ranero, C., Sallares, V. (2017). Active tectonics of the Calabrian subduction revealed by new multi-beam bathymetric data and high resolution seismic profiles in the Ionian Sea (Central Mediterranean). *Earth and Planetary Science Letters*. 461, 61-72. doi:10.1016/j.epsl.2016.12.020.

Handy, M. R., Schmid, S. M., Bousquet, R., Kissling, E., & Bernoulli, D. (2010). Reconciling plate-tectonic reconstructions of Alpine Tethys with the geological–geophysical record of spreading and subduction in the Alps. *Earth-Science Reviews*, *102*(3-4), 121-158.

Heit, B., F. d. L. Mancilla, X. Yuan,J. Morales, D. Stich, Martín, R., andA. Molina-Aguilera (2017). Tearing of the mantle lithosphere along the intermediate-depth seismicity zone beneath the Gibraltar Arc: The onset of lithospheric delamination, *Geophys. Res. Lett.*, 44, 4027-4035, doi:10.1002/2017GL073358.

Heuret, A., & Lallemand, S. (2005). Plate motions, slab dynamics and back-arc deformation. *Physics of the Earth and Planetary Interiors*, *149*(1-2), 31-51.

Hirn, A., Nicolich, R., Gallart, J., Laigle, M., Cernobori, L., & ETNASEIS Scientific Group.

(1997). Roots of Etna volcano in faults of great earthquakes. *Earth and Planetary Science Letters*, *148*(1-2), 171-191.

Ike, T., Moore, G. F., Kuramoto, S. I., Park, J. O., Kaneda, Y., & Taira, A. (2008). Variations in sediment thickness and type along the northern Philippine Sea Plate at the Nankai Trough. *Island Arc*, *17*(3), 342-357.

Jacques, E., Monaco, C., Tapponnier, P., Tortorici, L., & Winter, T. (2001). Faulting and earthquake triggering during the 1783 Calabria seismic sequence. *Geophysical Journal International*, *147*(3), 499-516.

Jolivet, L., Faccenna, C., Agard, P., Frizon de Lamotte, D., Menant, A., Sternai, P., & Guillocheau, F. (2015). Neo-Tethys geodynamics and mantle convection: from extension to compression in Africa and a conceptual model for obduction. *Canadian journal of earth sciences*, *53*(11), 1190-1204.

Kastens, K. A. (1991). Rate of outward growth of the Mediterranean Ridge accretionary complex. *Tectonophysics*, *199*(1), 25-50.

Klingelhoefer, F., Gutscher, M. A., Ladage, S., Dessa, J. X., Graindorge, D., Franke, D., ... & Chauhan, A. (2010). Limits of the seismogenic zone in the epicentral region of the 26 December 2004 great Sumatra-Andaman earthquake: Results from seismic refraction and wide-angle reflection surveys and thermal modeling. Journal of Geophysical Research: Solid Earth, 115(B1).

Koulali, A., Ouazar, D., Tahayt, A., King, R.W., Vernant, P., Reilinger, R.E., McClusky, S., Mourabit, T., Davila, J.M., Amraoui, N. (2011). New GPS constrains on active deformation along the Africa–Iberia plate boundary. *Earth Planet. Sci. Lett*.308 (1), 211–217. doi.org/10.1016/j.epsl.2011.05.048.

Krien, Y., & Fleitout, L. (2008). Gravity above subduction zones and forces controlling plate motions. *Journal of Geophysical Research: Solid Earth*, *113* (B9).

Lallemand, S., Heuret, A., & Boutelier, D. (2005). On the relationships between slab dip, back-arc stress, upper plate absolute motion, and crustal nature in subduction zones. *Geochemistry, Geophysics, Geosystems*, *6*(9).

Le Meur, E., Virieux, J., & Podvin, P. (1997). Seismic tomography of the Gulf of Corinth: a comparison of methods.

Levitt, D. A., & Sandwell, D. T. (1995). Lithospheric bending at subduction zones based on depth soundings and satellite gravity. *Journal of Geophysical Research: Solid Earth*, *100*(B1), 379-400.

Loureiro, A., Afilhado, A., Matias, L., Moulin, M., & Aslanian, D. (2016). Monte Carlo approach to assess the uncertainty of wide-angle layered models: Application to the Santos Basin, Brazil. *Tectonophysics*, *683*, 286-307.

Ludwig, W. J., Nafe, J. E., & Drake, C. L. (1970). The Sea, Vol. 4, Part 1.

Maesano, F. E., Tiberti, M. M., & Basili, R. (2017). The Calabrian Arc: three-dimensional modeling of the subduction interface. *Scientific reports*, *7*(1), 8887.

Makris, J., Nicolich, R., & Weigel, W. (1986). A seismic study in the western Ionian Sea. In *Annales geophysicae. Series B. Terrestrial and planetary physics* (Vol. 4, No. 6, pp. 665-678).

Marani, M. P., & Trua, T. (2002). Thermal constriction and slab tearing at the origin of a superinflated spreading ridge: Marsili volcano (Tyrrhenian Sea). *Journal of*

*Geophysical Research: Solid Earth*, *107*(B9), EPM-3.

Marotta, M. A., Spelta, E., & Rizzetto, C. (2006). Gravity signature of crustal subduction inferred from numerical modelling. *Geophysical Journal International*, *166*(2), 923-938.

Medaouri, M., Déverchère, J., Graindorge, D., Bracene, R., Badji, R., Ouabadi, A., ... & Bendiab, F. (2014). The transition from Alboran to Algerian basins (Western Mediterranean Sea): chronostratigraphy, deep crustal structure and tectonic evolution at the rear of a narrow slab rollback system. *Journal of Geodynamics*, 77, 186-205.

Minelli, L., & Faccenna, C. (2010). Evolution of the Calabrian accretionary wedge (central Mediterranean). *Tectonics*, *29*(4).

Moretti, I., & Royden, L. (1988). Deflection, gravity anomalies and tectonics of doubly subducted continental lithosphere: Adriatic and Ionian Seas. *Tectonics*, *7*(4), 875-893.

Moscoso, E., Grevemeyer, I., Contreras-Reyes, E., Flueh, E. R., Dzierma, Y., Rabbel, W., & Thorwart, M. (2011). Revealing the deep structure and rupture plane of the 2010 Maule, Chile earthquake (Mw= 8.8) using wide angle seismic data. *Earth and Planetary Science Letters*, *307*(1-2), 147-155.

Mueller, R. D., W. R. Roest, J.-Y. Royer, L. M. Gahagan, and J. G. Sclater (1997). Digital isochrons of the world's ocean floor, *J. Geophys. Res.*, 102, 3211–3214, doi:10.1029/ 96JB01781.

Neri, G., B. Orecchio, C. Totaro, G. Falcone, and D. Presti (2009). Subduction beneath Southern Italy close the ending: Results from seismic tomography, *Seismol. Res. Lett*., 80(1), 63–70, doi:10.1785/gssrl.80.1.63.

Neri, G., Marotta, A. M., Orecchio, B., Presti, D., Totaro, C., Barzaghi, R., & Borghi, A. (2012). How lithospheric subduction changes along the Calabrian Arc in southern Italy: geophysical evidences. *International Journal of Earth Sciences*, *101*(7), 1949-1969.

Nicolich, R., Laigle, M., Hirn, A., Cernobori, L., & Gallart, J. (2000). Crustal structure of the Ionian margin of Sicily: Etna volcano in the frame of regional evolution. *Tectonophysics*, *329*(1-4), 121-139.

Oleskevich, D. A., Hyndman, R. D., & Wang, K. (1999). The updip and downdip limits to great subduction earthquakes: Thermal and structural models of Cascadia, south Alaska, SW Japan, and Chile. *Journal of Geophysical Research: Solid Earth*, *104*(B7), 14965-14991.

Palano, M., L. Ferranti, C. Monaco, M. Mattia, M. Aloisi, V. Bruno, F. Cannavò, and G. Siligato (2012). GPS velocity and strain fields in Sicily and southern Calabria, Italy: Updated geodetic constraints on tectonic block interaction in the central Mediterranean, *J. Geophys. Res.*, 117, B07401, doi:10.1029/2012JB009254.

Palano, M., Gonzalez, P.J. and Fernandez, J. (2015). The Diffuse Plate boundary of Nubia and Iberia in the Western Mediterranean: Crustal deformation evidence for viscous coupling and fragmented lithosphere. *Earth and Planetary Science Letters*, 430. pp. 439-447, doi:10.1016/j.epsl.2015.08.040

Palano, M., C. Piromallo, and C. Chiarabba (2017). Surface imprint of toroidal flow at retreating slab edges: The first geodetic evidence in the Calabrian subduction system, Geophys. Res. Lett., 44, doi:10.1002/ 2016GL071452.

Pavlis, N. K., Holmes, S. A., Kenyon, S. C., & Factor, J. K. (2012). The development and evaluation of the Earth Gravitational Model 2008 (EGM2008). *Journal of geophysical research: solid earth*, *117*(B4).

Piana Agostinetti, N., Steckler, M. S., & Lucente, F. P. (2009). Imaging the subducted slab under the Calabrian Arc, Italy, from receiver function analysis. *Lithosphere*, *1*(3), 131-138.

Piatanesi, A., & Tinti, S. (1998). A revision of the 1693 eastern Sicily earthquake and tsunami. *Journal of Geophysical Research: Solid Earth*, *103*(B2), 2749-2758.

Polonia, A., Torelli, L., Mussoni, P., Gasperini, L., Artoni, A., & Klaeschen, D. (2011). The Calabrian Arc subduction complex in the Ionian Sea: Regional architecture, active deformation, and seismic hazard. *Tectonics*, *30*(5).

Rosenbaum, G., Lister, G. S., & Duboz, C. (2002). Reconstruction of the tectonic evolution of the western Mediterranean since the Oligocene. *Journal of the Virtual Explorer*, *8*, 107-130.

Sallares, V., Gailler, A., Gutscher, M.-A., Graindorge, D., Bartolome, R., Gracia, E., Diaz, J., and Zitellini, N. (2011). Seismic evidence for the presence of Jurassic oceanic crust in the central Gulf of Cadiz (SW Iberia). *Earth and Planetary Science Letters*, v. 311, p. 112-123, doi:10.1016/j.epsl.2011.09.003.

Sarkar, A., Nunn, J. A., & Hanor, J. S. (1995). Free thermohaline convection beneath allochthonous salt sheets: an agent for salt dissolution and fluid flow in Gulf Coast sediments. Journal of Geophysical Research: Solid Earth, 100(B9), 18085-18092.

Scarfì, L., Messina, A., & Cassisi, C. (2013). Sicily and southern Calabria focal mechanism database: a valuable tool for local and regional stress-field determination. *Annals of Geophysics*, *56*(1), 0109.

Scarfì, L., Barberi, G., Musumeci, C. & Patanè, D. (2016). Seismotectonics of northeastern Sicily and southern Calabria (Italy): New constraints on the tectonic structures featuring in a crucial sector for the central Mediterranean geodynamics. Tectonics 35, 812–832, https://doi.org/10.1002/2015TC004022.

Scarfì, L., Barberi, G., Barreca, G., Cannavò, F., Koulakov, I., & Patanè, D. (2018). Slab narrowing in the Central Mediterranean: the Calabro-Ionian subduction zone as imaged by high resolution seismic tomography. *Scientific reports*, *8*(1), 5178. doi: 10.1038/s41598-018-23543-8

Scarpa, R. (1982). Travel-time residuals and three-dimensional velocity structure of Italy. *pure and applied geophysics*, *120*(3), 583-606.

Schellart, W. P. (2004), Kinematics of subduction and subduction-induced flow in the upper mantle, J. Geophys. Res., 109, B07401, doi:10.1029/2004JB002970.

Selvaggi, G., & Chiarabba, C. (1995). Seismicity and P-wave velocity image of the Southern Tyrrhenian subduction zone. *Geophysical Journal International*, *121*(3), 818-826.

Séranne, M. (1999). The Gulf of Lion continental margin (NW Mediterranean) revisited by IBS: an overview. Geological Society, London, Special Publications, 156(1), 15-36.

Schmidt, S., Plonka, C., Gotze, H. J., & Lahmeyer, B. (2011). Hybrid modeling of gravity, gravity gradients and magnetic fields. *Geophysical Prospecting*, *59*(6), 1046-1051.

Spakman, W., & Wortel, R. (2004). A tomographic view on western Mediterranean geodynamics. In *The TRANSMED atlas. The Mediterranean region from crust to*

*mantle* (pp. 31-52). Springer, Berlin, Heidelberg.

Spakman, W., van der Lee, S., & van der Hilst, R. (1993). Travel-time tomography of the European-Mediterranean mantle down to 1400 km. *Physics of the Earth and Planetary Interiors*, *79*(1-2), 3-74.

Speranza, F., Maniscalco, R., & Grasso, M. (2003). Pattern of orogenic rotations in central–eastern Sicily: implications for the timing of spreading in the Tyrrhenian Sea. *Journal of the Geological Society*, *160*(2), 183-195.

Speranza, F., L. Minelli, A. Pignatelli, and M. Chiappini (2012). The Ionian Sea: The oldest in situ ocean fragment of the world?, J. Geophys. Res. 117, B12101, doi:10.1029/2012JB009475.

Underwood, M. B. (2007). Sediment inputs to subduction zones: Why lithostratigraphy and clay mineralogy matter. The seismogenic zone of subduction thrust faults.

van Hinsbergen, D. J. J., Mensink, M., Langereis, C. G., Maffione, M., Spalluto, L., Tropeano, M., & Sabato, L. (2014a). Did Adria rotate relative to Africa?. *Solid Earth*, *5*(2), 611-629.

van Hinsbergen, D. J. J., R. L. M. Vissers, and W. Spakman (2014b). Origin and consequences of western Mediterranean subduction, rollback, and slab segmentation, *Tectonics*, 33, 393-419, doi:10.1002/tect.20125.

Watts, A. B., J. P. Platt, and P. Buhl (1993). Tectonic evolution of the Alboran Sea Basin, *Basin Res.*, 5, 153–177, doi:10.1111/j.1365-2117.1993.tb00063.x.

Westaway, R. (1993). Quaternary uplift of southern Italy. *Journal of Geophysical Research: Solid Earth*, *98*(B12), 21741-21772.

White, R. S., McKenzie, D., & O'Nions, R. K. (1992). Oceanic crustal thickness from seismic measurements and rare earth element inversions. *Journal of Geophysical Research: Solid Earth*, *97*(B13), 19683-19715.

Wortel, M. J. R., & Spakman, W. (2000). Subduction and slab detachment in the Mediterranean-Carpathian region. *Science*, *290*(5498), 1910-1917.

Wortel, R., Govers, R., & Spakman, W. (2009). Continental collision and the STEP-wise evolution of convergent plate boundaries: From structure to dynamics. In *Subduction Zone Geodynamics* (pp. 47-59). Springer, Berlin, Heidelberg.Zelt, C. A., & Smith, R. B. (1992). Seismic traveltime inversion for 2-D crustal velocity structure. *Geophysical journal international*, *108*(1), 16-34.

Zelt, C. A. (1999). modeling strategies and model assessment for wide-angle seismic traveltime data. *Geophysical Journal International*, *139*(1), 183-204.

Zelt, C. A., & Smith, R. B. (1992). Seismic traveltime inversion for 2-D crustal velocity structure. *Geophysical journal international*, *108*(1), 16-34.

Zito, G., Mongelli, F., De Lorenzo, S., & Doglioni, C. (2003). Heat flow and geodynamics in the Tyrrhenian Sea. Terra Nova, 15(6), 425-432.

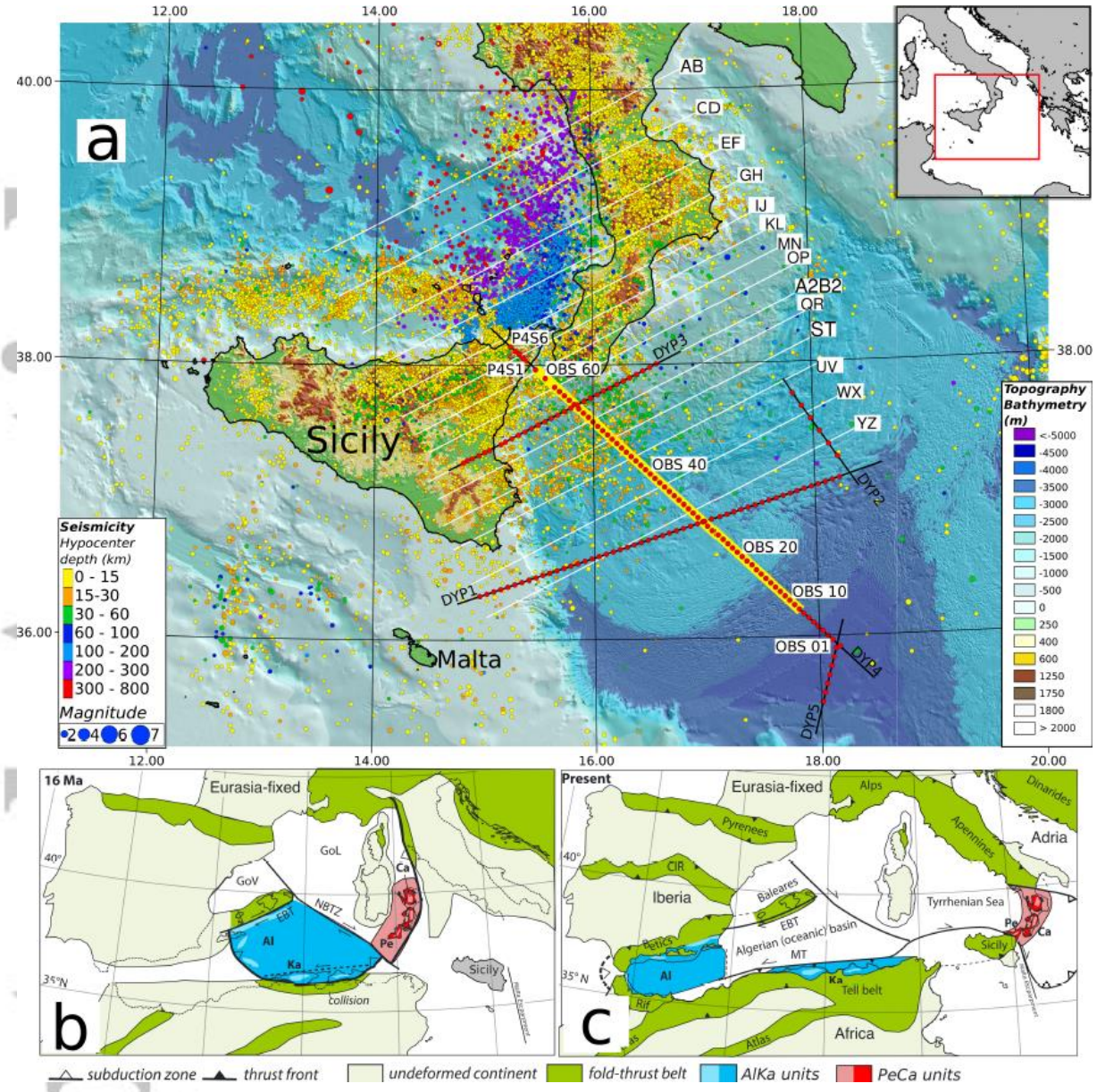


Figure 1: (a) Location map of the study area. Ocean bottom seismometers and landstations deployed during the Dionysus cruise (Oct.-Nov. 2014, Meteor).. Earthquakes from the INGV-ISIDe catalogue (http://cnt.rm.ingv.it/en) are plotted with a size proportional to the magnitude and color corresponding to the hypocenter depth. The CROP-M3 MCS profile is coincident with DY-P4 and marked by underlying bold yellow line (Figure 5 this study and shown in detail inPolonia et al., 2011). Profiles used for the construction of the gravity model are marked by white lines. Bathymetry from Gutscher et al., 2017 and EMODNET. (b) and (c) Paleogeographic reconstruction figures are modified from van Hinsbergen et al., 2014a. Al = Alboran; Ca = Calabria; CIR = Central Iberian Ranges; EBT = Emile Baudot Transform; GoL = Gulf of Lion; GoV = Gulf of Valencia; Ka = Kabylides; NBTZ = North Balearic Transform Zone; Pe = Peloritan Mountains. Inset shows the location of the study are in the central Mediterranean region.

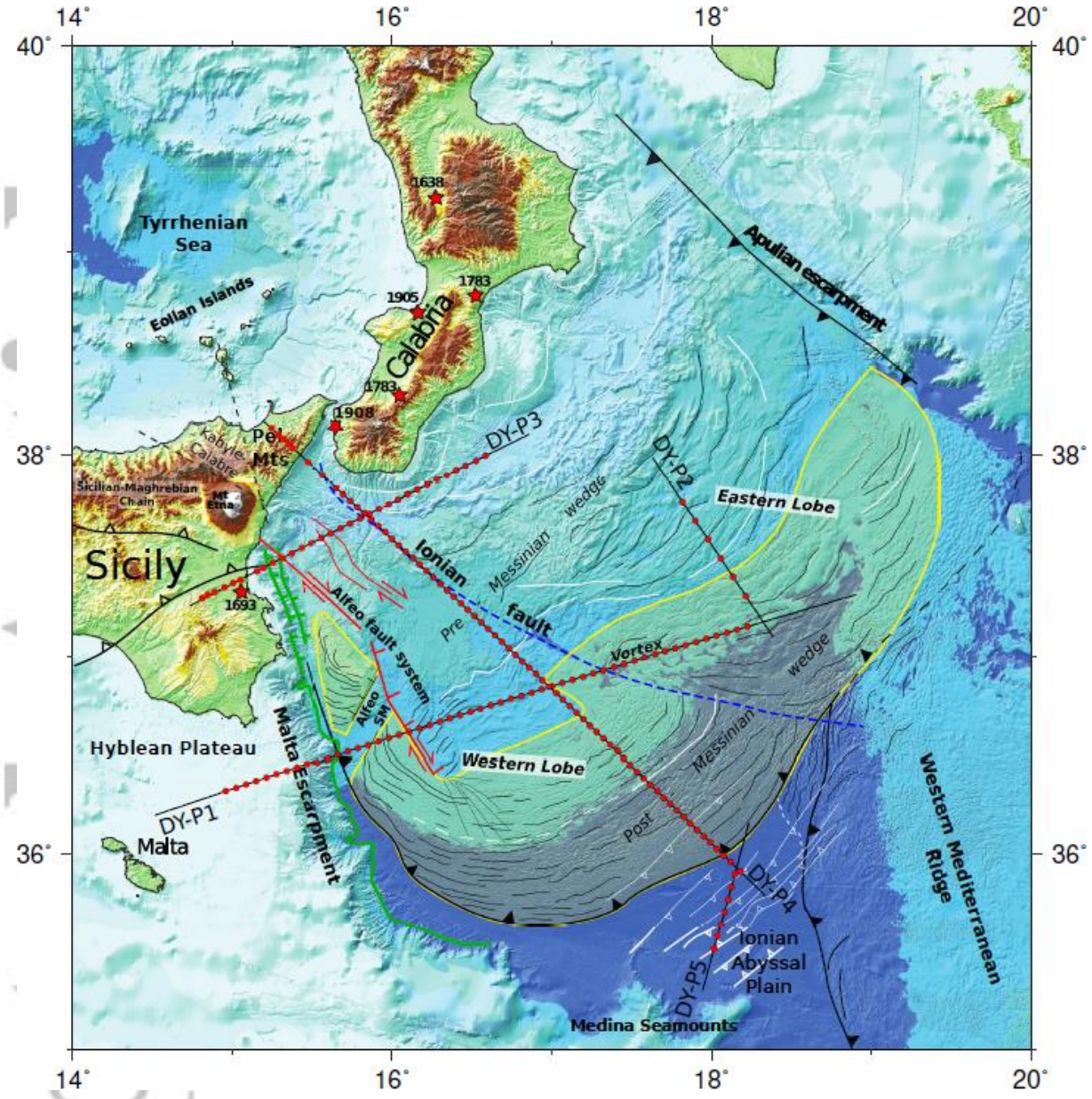


Figure 2: Tectonic map of the study area. Ocean bottom seismometers and landstations are marked by red dots. Red stars mark hypocenters location of historical earthquakes. CROP-M3 MCS profile is coincident to DY-P4 (Figure 5; Polonia et al., 2011). Bathymetry from Gutscher et al., 2017. (After Dellong et al., 2018). Yellow shaded area marks the supposed extension of tectonically thickened evaporites in the Calabrian accretionary wedge.

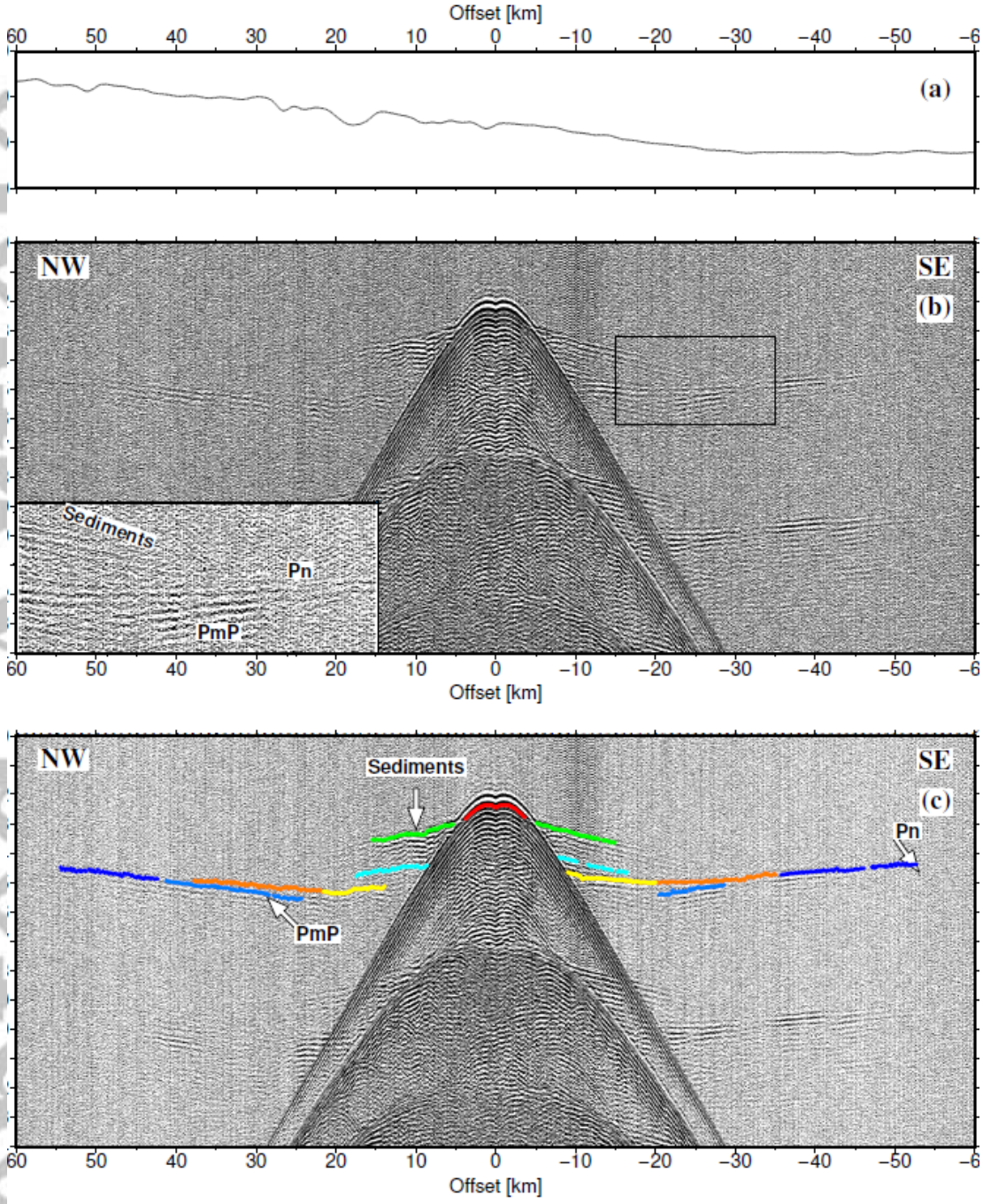


Figure 3: (a) Seafloor bathymetry along the sections shown below (b) Data section from OBS 08 vertical geophone channel. The data are bandpass filtered (3-4-24-36 Hz corner frequencies) and reduced to a velocity of 6 km/s (c) Data section OBS 08 with travel-time picks overlain.

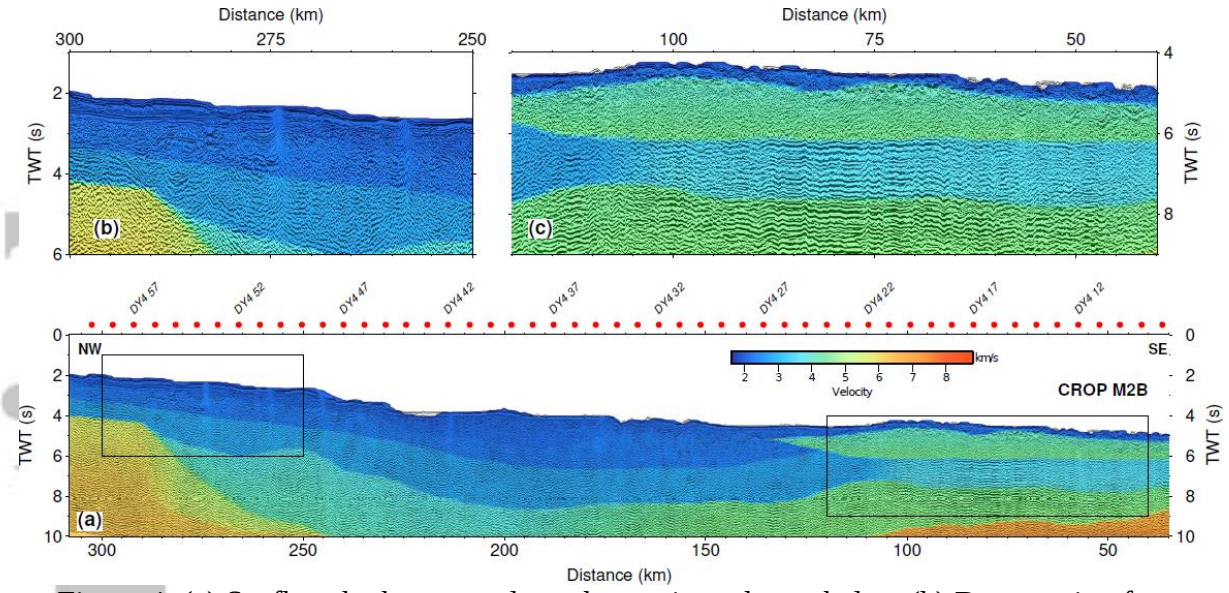


Figure 4: (a) Seafloor bathymetry along the sections shown below (b) Data section from landstation S3 vertical geophone channel. The data are bandpass filtered (3-4-24-36 Hz corner frequencies) and reduced to a velocity of 6 km/s (c) Data section from landstation S3 with travel-time picks overlain.

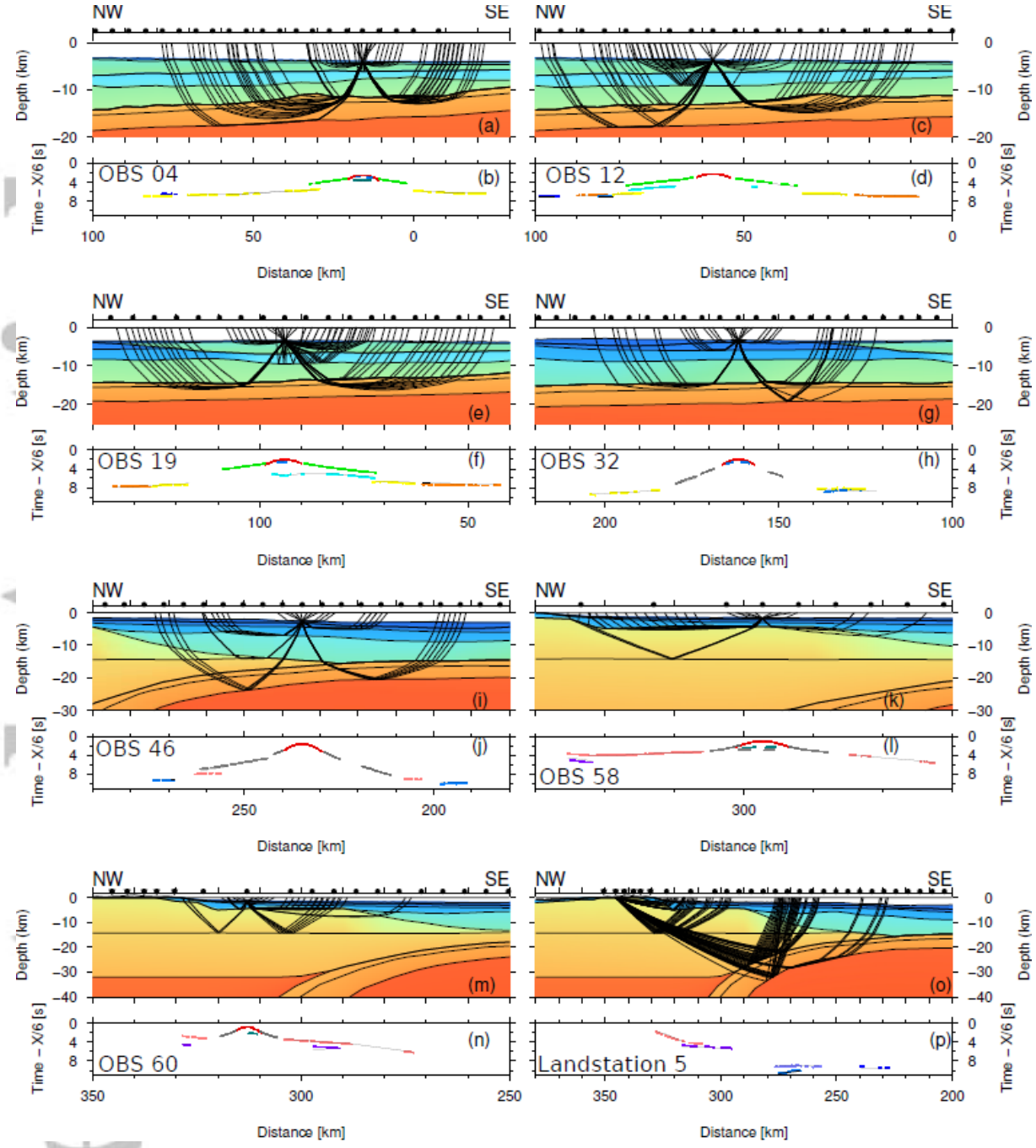


Figure 5: (a) Reflection seismic section of the coincident CROP M2B profile (Polonia et al., 2011) with velocities from our wide-angle seismic model underlain (see Figure 7). OBS locations are marked by red circles. (b) and (c) are zooms indicated on (a) to show more details of the reflection seismic data.

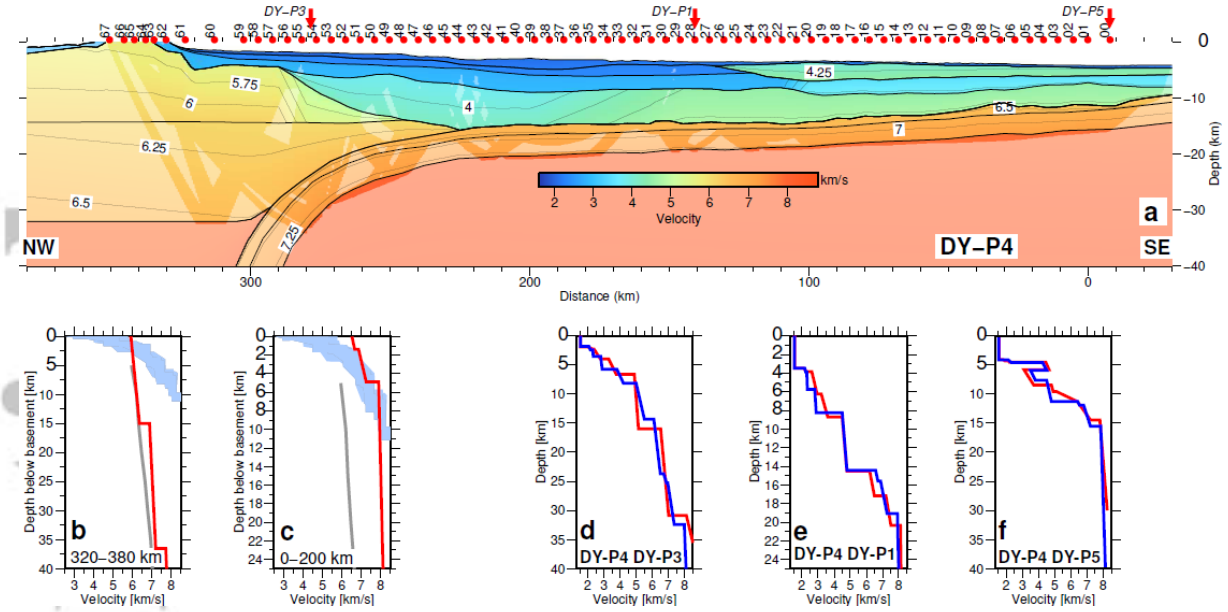


Figure 6: Panels a,c,e,g,i,k,m,o model layers and raypaths of every 10th ray and panels b, d,f,h,j,l,n,p corresponding travel-time picks and predicted arrivals (black lines). OBS positions are marked in the lower panels.

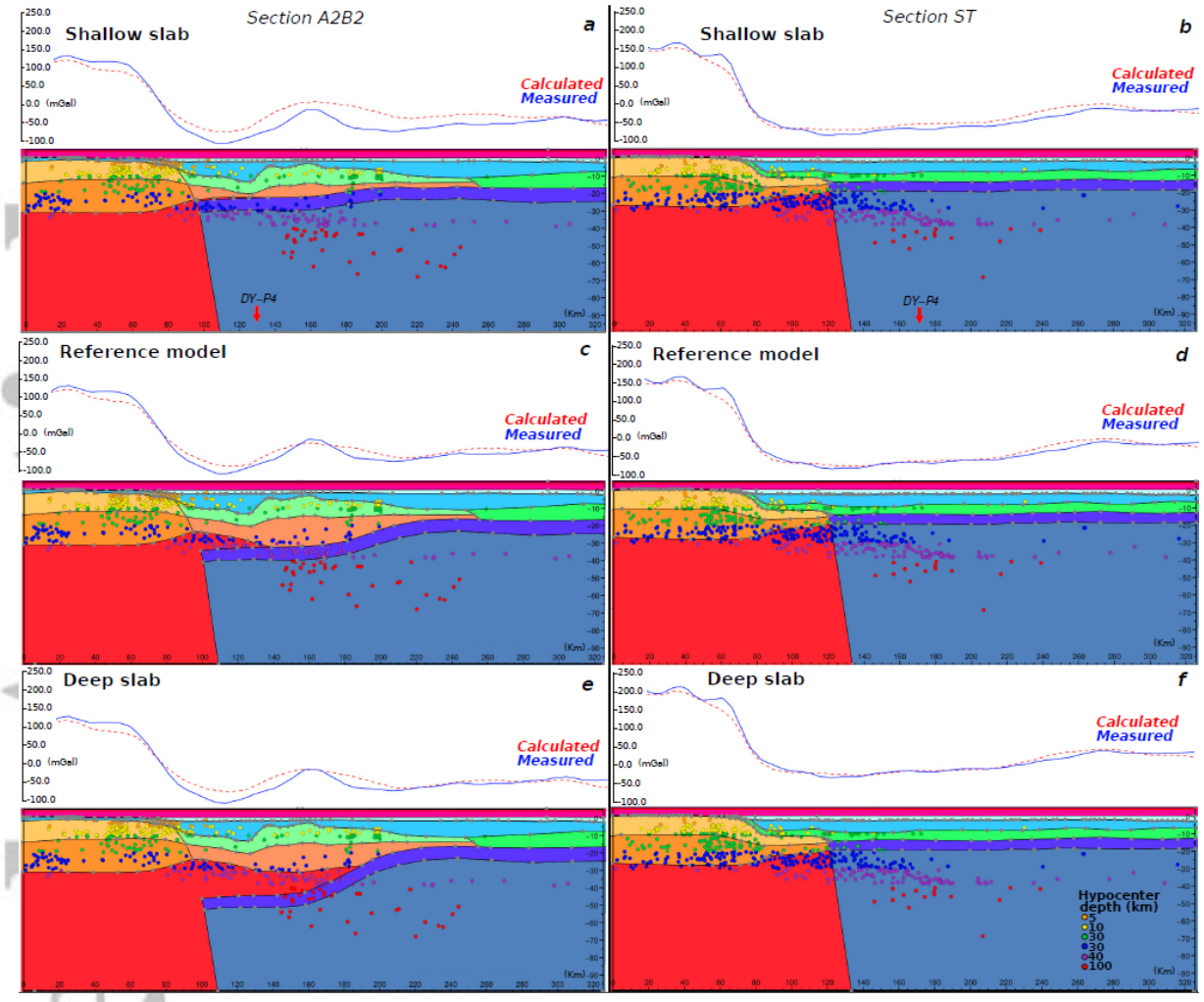


Figure 7: (a) Final velocity model of the profile DY-P4. The velocities are contoured every 0.25 km/s and shaded areas are constrained by rays. Red dots mark the position of the seafloor instruments and arrows mark the crossing points with DY-P1 and DY-P3 profiles. (b) and (c) Averaged velocity-depth profiles underneath the basement for the Ionian basin and the Sicily crust. Blue envelope represents the velocity compilation for Atlantic oceanic crust from White et al., 1992 and gray thick line the velocity compilation for extended continental crust from Christensen and Mooney, 1995 (d), (e) and (f) Velocity depth profiles at the crossing. Red line is the DY-P4 profile and blue lines trace the DY-P1 and DY-P3 profiles.

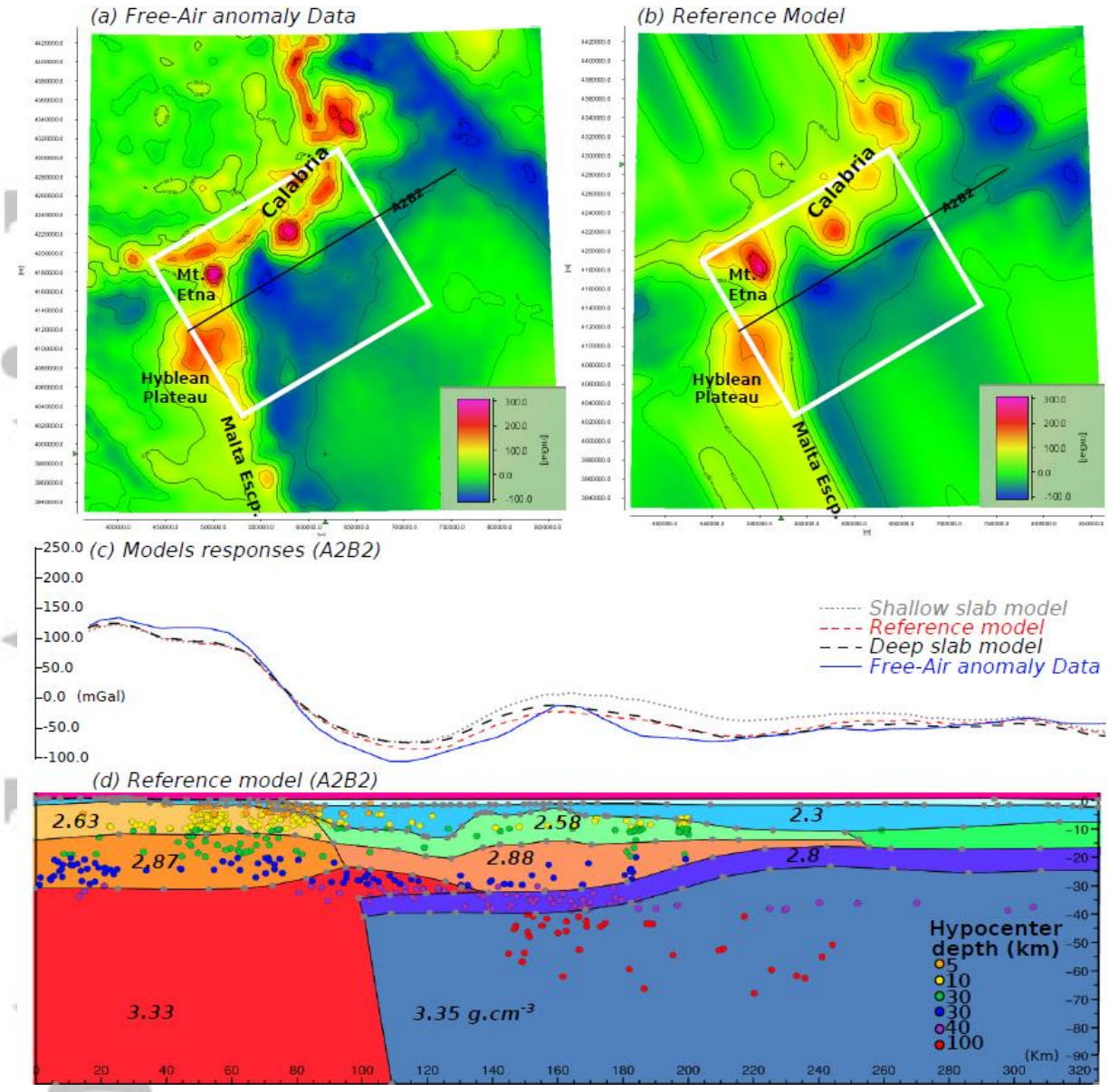


Figure 8: (a) Map of the Free-air gravity anomaly (WGM-2012 – Bonvalot et al., 2012; Pavlis et al., 2012) (b) 3D Reference model gravity response. White rectangle shows the area of interest around the A2B2 profile (black line). (c) Gravity response of the different 3D models (solely varying the oceanic slab depth) along the A2B2 profile. (d) A2B2 cross-section extracted from the Reference model, showing each individual layers and their densities. Earthquake hypocenters, projected from 10 km onto the profile, are shown by small circles colored by depth.

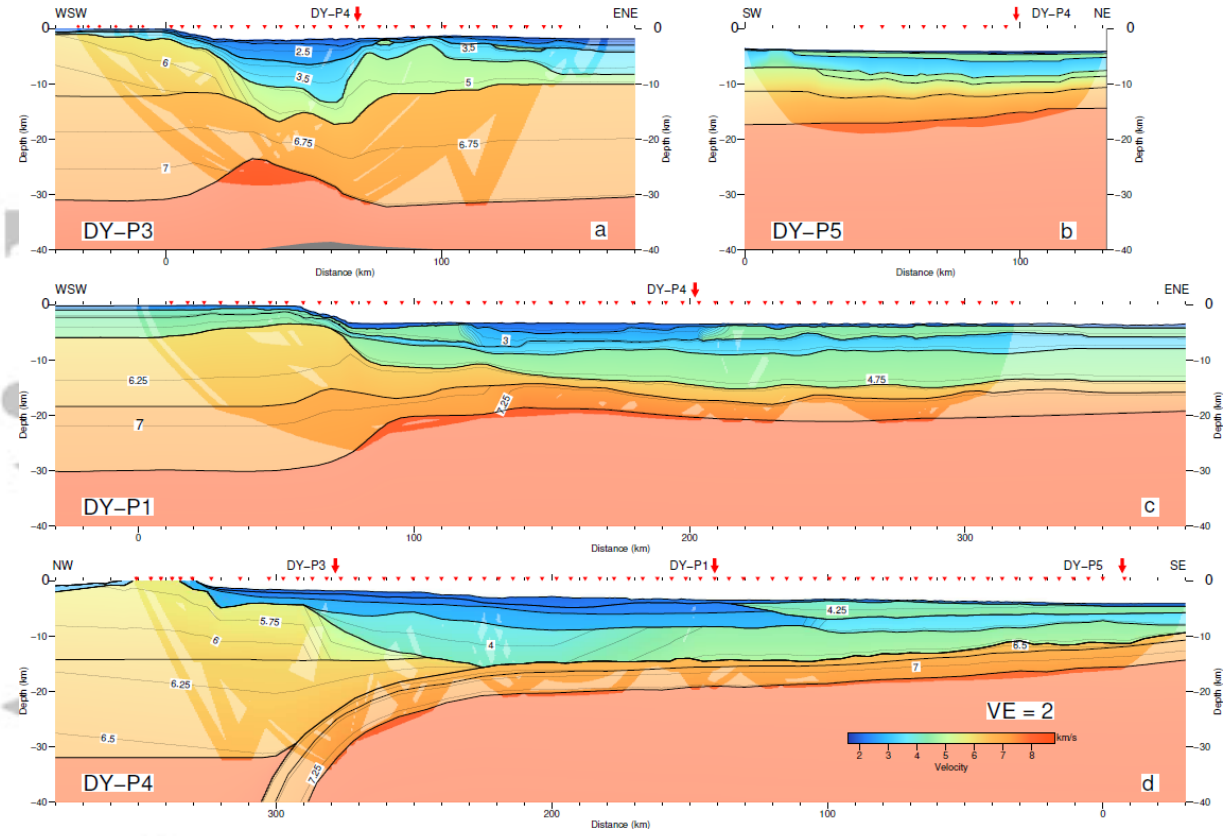


Figure 9: Final velocity models of the wide-angle seismic profiles DY-P3 (a), DY-P5 (b), DY-P1 (c) and DY-P4 (d) Crossings between profiles are marked by red arrows and OBS positions by inverted triangles. Vertical exaggeration is 2.

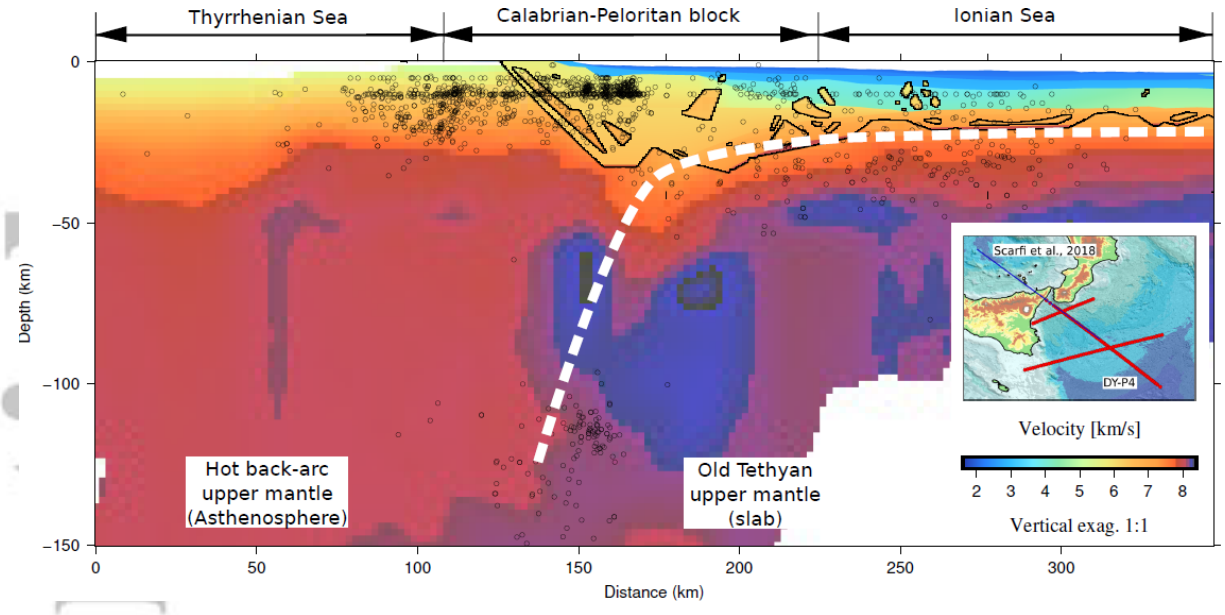


Figure 10: Profile extracted from the tomographic model of (Scarfi et al. 2018) with layer boundaries from the DY-P4 profile overlain. Earthquakes projected from a maximum of 5 km distance along the profile are marked as black dots. P-wave velocities in the model are indicated by the scale at right (in the inset). Inset: Bathymetry of the study region (Gutscher et al, 2017). Blue line shows position of the tomography model and red dots OBS positions.

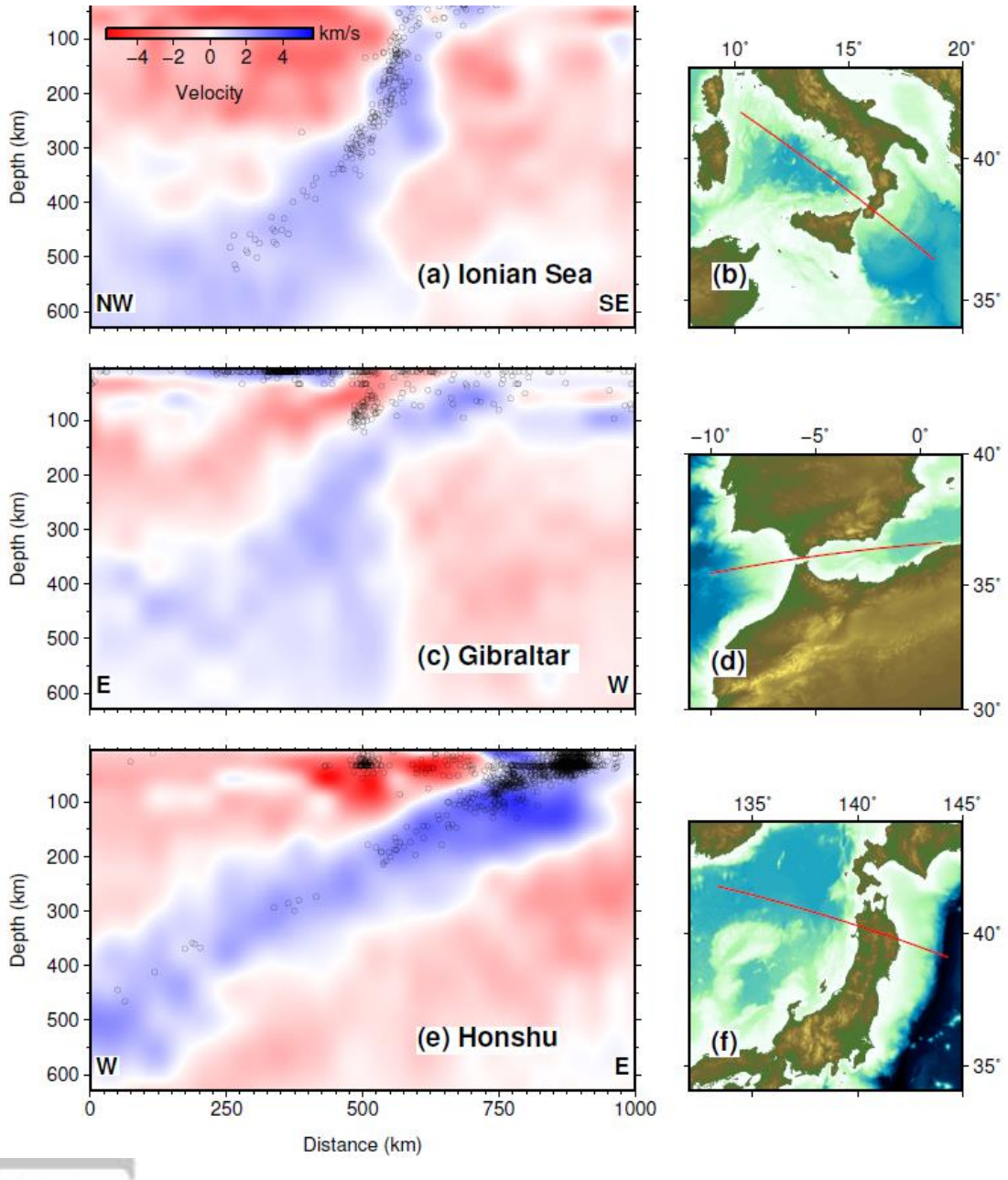


Figure 11: (a) Cross-section in the global earthquake traveltime tomographic model UU-P07 (Amaru, 2007) through the Ionian sea subduction zone. (b) Location map for the profile in panel (a). (c) Cross-section in the UU-P07 tomographic model (Amaru, 2007) through the Gibraltar subduction zone. (d) Location map for the profile in panel (c). (e) Cross-section in the UU-P07 (Amaru, 2007) through the Honshu subduction zone. (f) Location map for the profile in panel (e).

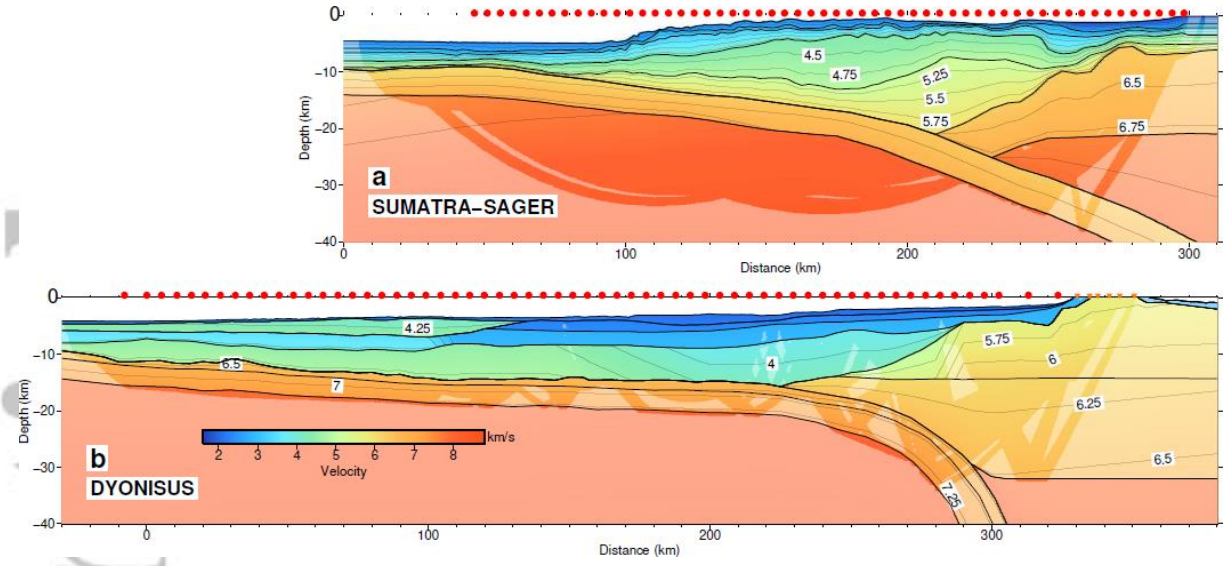


Figure 12: Comparison of the wide-angle seismic profiles from the (a) Sumatra SAGER cruise (Klingelhoefer et al., 2009) showing gradual flexure and a marked bulge expressed as a basement high around 40 km profile distance and (b) DYONISUS DY-P4 showing a nearly constant extremely shallow plate dip (1 – 2°) and then a slab hinge between 250 and 300 km profile distance where the slab dip increases abruptly to >45°.

*Table 1: Name, phase number and RMS error for all phases.*

| Phase | Phase Number | Number of picks | RMS error [ms] |
|---|---|---|---|
| Water | 1 | 3879 | 0.030 |
| Sediment 1 | 2 | 1133 | 0.129 |
| Sediment 2 | 3 | 3616 | 0.079 |
| Sediment 3 | 9 | 823 | 0.190 |
| Sediment 4 | 18 | 659 | 0.136 |
| Sediment 5 | 16 | 306 | 0.162 |
| Sediment reflection 1 | 4 | 676 | 0.107 |
| Sediment reflection 2 | 5 | 326 | 0.086 |
| Sediment refllection 3 | 10 | 102 | 0.193 |
| Sediment reflection 4 | 19 | 1815 | 0.142 |
| Top basement | 6 | 1469 | 0.178 |
| Oceanic lower crust | 15 | 3494 | 0.139 |
| Continental lower crust | 11 | 3039 | 0.147 |
| Intra-crustal reflection | 12 | 506 | 0.229 |
| PmP continental | 7 | 422 | 0.203 |
| PmP oceanic | 14 | 811 | 0.189 |
| Pn | 8 | 895 | 0.086 |
| All phases | | 23971 | 0.133 |